Theor Chem Acc (2002) 108:187–213
DOI 10.1007/s00214-002-0368-4

Theoretical
Chemistry Accounts

Feature article

A priori rate constants for kinetic modeling

R. Sumathi, William H. Green Jr.

Department of Chemical Engineering, Massachusetts Institute of Technology, Cambridge, MA 02139, USA

Received: 6 February 2002 / Accepted: 2 June 2002 / Published online: 2 October 2002
© Springer-Verlag 2002

Abstract. The advent of computer-aided methods for constructing detailed kinetic models of multicomponent reacting systems provides fresh motivation for the development of efficient and accurate methods for estimating rate constants. There is now the real likelihood that a priori rate estimates, formerly of primarily academic interest, could directly impact major public policy and business decisions. This opportunity brings many challenges. The process of building a computer model for a real-world system can require hundreds of thousands of rate estimates, making most existing rate calculation techniques impractical. Also, the demands for tight error bars on model predictions used to make major decisions often imply levels of accuracy unachievable with existing rate calculation techniques. Past and recent progress towards developing fast and accurate rate estimates is selectively reviewed, and our methodology is outlined. New rate estimates for several types of reactions involving O and HO_2 are presented. Several technical issues requiring further work by the theoretical chemistry community are highlighted. Electronic supplementary material to this paper can be obtained by using the Springer Link server located at http://dx.doi.org/10.1007/s00214-002-0368-4.

Key words: Abstraction reaction – Group additivity – $O + RH - HO_2 + R - H + ROCH_3$

1 Introduction

1.1 Motivation

For many years, chemists have worked to develop accurate methods for estimating reaction rate constants a priori. The main motivation for this line of research was to check our understanding of the fundamentals of reactive chemistry.

For many decades, this research was primarily empirical or semiempirical, using tools such as Hammett correlations [1] and Benson's thermochemical kinetics (TK) [2] concepts to understand experimentally observed trends in reactivity. These methods have been demonstrated to be very accurate if sufficient experimental data on similar reactions have been collected, but their predictions are only qualitative for data-poor situations. Most of these methods were developed long before modern computers and algorithms made it possible to solve stiff chemical kinetic simulations or to calculate reaction rates a priori.

Over the past 2 decades, quantum chemical methods, computer hardware, and rate theory have improved to the extent that one can fairly accurately predict reaction rates a priori, without reliance on extensive experimental correlations or qualitative rate-estimation procedures [3, 4]. At the same time, the technology for handling and solving chemical kinetic simulations has also improved dramatically (VODE [5], DASSL [6], CHEMKIN [7]). These improvements allow us to move beyond the fundamentals of rate estimation towards the application of these a priori rates for predicting the behavior of technologically important systems such as partial oxidation, combustion, and pyrolysis. These systems are often very complex, with many simultaneously reacting species, numerous undetected reactive intermediates, and often the chemistry is strongly coupled to heat and mass transport.

To deal with this complexity, a computer is used both to construct the simulation and to solve it. Large chemical kinetic models can be generated rapidly by the computer, and often these comprehensive computer models identify kinetically significant species and reactions missed when models are constructed by hand. However, the cost of this comprehensiveness is that during the model construction process thousands or even millions of rate constants must be estimated a priori. (Fortunately most of these are found to be

Correspondence to: W.H. Green Jr.
e-mail: whgreen@mit.edu

Electronic supplementary material to this paper can be obtained by using the Springer LINK server located at http://dx.doi.org/10.1007/s00214-002-0368-4

negligible under the particular reaction conditions of interest.) Several software packages for constructing kinetic models automatically have now been developed [8–35], and they are reviewed and detailed elsewhere [36]. Some algorithms for selecting the species and reactions to be included in the kinetic model significantly reduce the number of rate constants which must be estimated without missing any important steps, but even the best existing species-selection algorithms require a very large number of rate estimates to ensure that no important reaction is missed [8, 13]. All existing model-construction algorithms are based on thermal rate constants, and so run into difficulties dealing with chemically activated reactions [37, 38, 39]. Computerized kinetic model generation is a relatively new field, and significant progress is being made on several fronts [40].

1.2 Overview of this article

The present article is focused on rate constant estimation processes fast enough and accurate enough to be appropriate for this challenging task. Note that the number of possible reactions rises superlinearly with the number of species in a reacting mixture, and exponentially with the size of the molecules involved, leading to a "combinatorial explosion" in the number of distinct rate estimates required. So only very fast automated procedures are practical – we will not be able to afford accurate quantum chemical calculations on every reaction, nor expensive quantum-scattering calculations described in Sect. 1.3 on every reaction. Even the reaction-class transition-state theory (TST) of Truong et al [41, 42] discussed in Sect. 1.5, which is philosophically similar to the methods we propose, is not feasible for this application, since it requires performing single-point transition-state (TS) barrier calculations for each reaction. (However, the approach of Truong et al. or something similar may well be appropriate for refinement of the rate estimates for the most important reactions.)

The key to making these many rate estimates is to classify similar reactions together into "reaction families". High-quality calculations and/or experimental data are made on a few members of each family, and these results can be used to derive rules for rather accurately predicting the rates of other members.

The most common approach, one taught in essentially all organic chemistry textbooks, and briefly reviewed in Sect. 1.4, is to classify reactions according to the functional groups that are actively involved. Some important reaction types for free-radical chemistry include hydrogen abstraction (a.k.a metathesis), radical addition to multiple bonds, recombination and disproportionation of radicals, and the reverse of each process. If one knows more about the reaction, one can obtain more precise predictions by subdividing these very broad reaction families according to the nearby (or even more distant) substituents on each of the active functional groups.

All modern rate-estimation methods are based either on experimental rate data, which unfortunately are usually scarce, or on (hopefully) high-accuracy first-principles rate calculations. We very briefly summarize methods used for these calculations, then selectively review less-computer-intensive rate-estimation methods in Sect. 1. We present our approach for building an automated fast rate-estimation method based on a few high-accuracy ab initio calculations in Sect. 2, and present some illustrative applications of our methodology to various reaction families in Sect. 3.

The present work is focused on gas-phase reactions on electronic ground states of relatively small neutral molecules, an important class of relatively well understood reactions. Considerable work on estimating the rates of condensed-phase macromolecular, photochemical, and ionic reactions will ultimately be required in order to allow accurate detailed modeling of the wide range of systems important in the environment, in biology, and in industry.

1.3 Reaction rates from first principles

Before presenting our rate-estimation method, we summarize briefly the improvements in quantum chemical methods and rate theories that make accurate a priori gas-phase rate predictions an achievable and realistic task. There have been many improvements in quantum chemistry, i.e., methods for computing and characterizing stationary points on potential-energy surfaces (PES), in methods for computing reaction rates that go beyond conventional TST, including barrierless reactions, and in methods for handling tunneling. There has also been some progress in improved methods for handling floppy modes, such as hindered internal rotations. Very recently there have also been significant improvements in the efficiency of methods for computing the pressure dependence of gas-phase reactions.

1.3.1 Quantum chemistry

In our view, the most important quantum chemistry development of the past decade is the introduction of accurate but affordable compound methods, where large effects are computed very accurately, and smaller terms are computed less precisely. Popular compound methods include the G family (G1 [43, 44], G2 [45], G2MP2 [46], G3 [47], G3MP2 [48], G3MP2B3 [49], G3B3 [49], G3S[50]), the complete-basis-set family (CBS-Q [51], CBS-APNO [52], CBS-RAD [53], CBS-QB3 [54]), the multicoefficient correlation (MC) methods [55, 56, 57] (MC-QCISD [58], MCG2[59], MCG3 [60]) and hybrid density functional theory (DFT)/Hartree–Fock (HF) methods [61] (e.g., B3LYP, BH&HLYP, MPW1K [62]). More expensive methods also use a similar approach, by combining a rather complicated treatment for some orbitals or configurations with a perturbative approach for others; notable examples include CCSD(T) [63], CAS-PT2 [64], MR-CI [65, 66], and Martin's W family [67, 68] of compound methods. The systems studied in the present work generally involve more than six heavy

atoms and at least nine valence electrons in lone-pair or half-occupied orbitals that must be included in the active space; because of the computational demands of these very high level methods it is not practical at present for us to use these approaches.

The G family uses a series of high level correlation calculations [e.g., QCISD(T), MP4, CCSD(T)] with moderate-sized basis sets to approximate the result of a more expensive calculation and includes, except for G3S, additive "higher-level correction" parameters that depend on the number of paired and unpaired electrons in the system. The central idea in the CBS methods is an extrapolation procedure to determine the projected second-order (MP2) energy in the limit of a CBS. MC methods combine scaling of the calculated energy, extrapolation to infinite basis set, and multiparameter fitting to a set of experimental data. DFT methods have recently evolved in a similar direction, with several parameters in proposed exchange–correlation functionals being adjusted to match experiment or high-level quantum calculations [69, 70, 71, 72, 73].

The compound methods make it practical to compute meaningful TSs for many individual reactions and allow critical evaluation of levels of accuracy achievable by different methods in computing the needed molecular parameters for TST calculations. These compound methods are now used routinely to calculate heats of reaction to within a few kilocalories per mole, and many spectroscopic constants to a few significant figures. It is not yet clear exactly how accurately one can calculate reaction barriers and TS properties: there are many examples in the literature demonstrating that these methods can work well for rate predictions, but also a few illustrating serious failures of various quantum methods. Usually these failures are thought to arise from problems with the underlying zero-order HF description, or possibly with the TS geometry (which is usually computed using a lower level of theory than the TS energy). For examples of these sorts of problems, see Sect. 3. Better methods for approximating high-level TS geometries would be very helpful, particularly for open-shell species; one proposed in the literature is the IRCMax method of Malick et al. [74].

A major part of the difficulty in establishing firm error bars on the quantum chemical TS calculations is that the barrier height is not directly observable, so one is often forced to try to back it out of the temperature (and possibly also pressure) dependence of the experimentally measured rate using some approximate model. Also, most quantum chemistry methods are based on single-configuration zero-order states, which are generally much more accurate for stable species than for TSs. In many cases, both the theoretical and the experimental barrier heights have very significant uncertainties, even when there is good experimental data on the rate constant measured at some particular temperature and pressure.

1.3.2 Internal rotors and other floppy modes

The conventional approach to computing thermochemistry and rates uses the harmonic oscillator approximation for the internal motions of the nuclei. However, in many cases the molecule or TS contains several internal degrees of freedom which are not well described as small amplitude harmonic oscillators. Uncertainties in how to treat these floppy modes often contribute significantly to the overall uncertainty in computed heat capacities and sometimes it is an important part of the uncertainty in rate constant calculations.

The most common type of floppy mode is internal rotation about each single bond between polyvalent atoms in a molecule. The partition function of a hindered rotor, Q_{hin}, depends upon the magnitude and shape of the hindrance potential. The most commonly adopted way to compute Q_{hin} for a one-dimensional symmetric hindered rotor is through the use of Pitzer–Gwinn tables [75, 76] which are compiled in terms of two dimensionless parameters, $1/Q_{\text{f}}$ and $V_0/\text{R}T$. Q_{f} is the free rotor partition function for the corresponding reduced moment of the rotating group, while V_0 is the rotational barrier height. Pitzer–Gwinn tables are highly appropriate for isolated and symmetric rotors revolving in a cosine potential.

Pitzer and Gwinn developed different approximations to account for the coupling of internal rotation with external rotation. In the case of multiple hindered rotors, they are coupled to each other in addition to their coupling with the principal axes of external rotation. Kilpatrick and Pitzer [77] developed protocols to calculate the average reduced moment of inertia by approximating the internal–internal and internal–external couplings. Furthermore, for systems with one or more asymmetric rotors, the external inertial tensor becomes a function of the internal rotation coordinates, and the rotation of one rotor (say, from a trans to a gauche conformation of an alkane) can very significantly change the moment of inertia of a second rotor. Nonetheless, in most published cases, a single I_{r} value has been used at all values of ϕ. Pilling and Robertson [78] treated the internal–external rotational couplings in butane and pentane within the approximation of classical mechanics.

Several groups have proposed approximate analytical formulae along the same lines as Pitzer's approach. Truhlar [79] provided an analytical form for Q_{hin} through a smooth hyperbolic interpolation function between the classical-harmonic-oscillator-partition-function limit at very low frequencies and the classical-free-rotor-partition-function limit at very low barriers. McClurg et al. [80] provided another analytical formula using a hindered-rotor density-of-states interpolation function based on the asymptotic behavior of the quantum mechanical partition function at low temperature and the classical partition function at high temperature. Ayala and Schlegel [81] proposed an analytical expression for Q_{hin} by approximating the Pitzer–Gwinn tables through polynomial functions of $(1/Q_{\text{f}})$ and $(V_0/k_{\text{B}}T)^{0.5}$. All the analytical forms approximate the hindrance to a cosine potential.

In reality, the internal rotors are not rigid. The first sign of this is that one usually computes significantly different $V(\phi)$ and V_0 depending on whether or not one optimizes (relaxes) the geometry at each ϕ_i. This

indicates that there is significant potential-energy coupling between ϕ and other internal coordinates, and that the rotor geometry varies with ϕ. If one looks carefully, one will also see that the vibrational frequencies of the small-amplitude vibrational modes also vary with ϕ. It is well known that one does much better in practice if one uses the relaxed $V(\phi)$, though of course this is much more expensive to compute since this requires a large number of quantum chemical geometry optimizations. To be consistent, one should also allow I_{hir} to vary with ϕ, and include various other terms in the one-dimensional effective Hamiltonian that reflects the kinetic energy coupling between the rotor and the small-amplitude vibrational modes. Work is in progress [82] to assess the importance of these terms and to develop an efficient method for computing Q_{hin} more accurately.

For convenience, the hindrance potentials of multiple rotors are almost always assumed to be independent of each other. It would be helpful to have criteria for deciding how much uncertainty is introduced by this assumption. East and Radom [83] performed essentially the only tests reported in the literature, using a two-dimensional ab initio potential. They demonstrated an improved accuracy in thermochemical predictions for systems with two internal rotors.

Often a hindered internal rotor is coupled to one or more nonrotor floppy large-amplitude motions, though few of these cases have been studied in any detail. The best experimental information is probably available from the high-resolution spectroscopy of the ethyl radical, which reveals the coupling between the large-amplitude umbrella vibration and the internal rotor [84]. Mazyar and Green [82] have computationally examined several cases where the TS geometry is sensitive to the orientation of a rotor, i.e., the reaction coordinate is coupled to the hindrance potential. Theoretical methods developed recently by Carter et al. [85] seem particularly appropriate for treating polyatomic systems with several strongly coupled large-amplitude motions.

1.3.3 Improved treatment of tunneling and TS recrossing

The present work and most rate calculations reported in the literature are based on conventional TST [86, 87, 88]. TST makes the quasiequilibrium thermodynamic approximation that the reactant maintains a Boltzmann energy distribution. The conventional TST model requires potential-energy information only at the reactant(s) and TS, a tremendous simplification obtained by treating many effects very approximately. In addition to the Born–Oppenheimer approximation, conventional TST assumes that one can identify a surface that cleanly separates reactants and products, that the lowest energy point on this dividing surface is the saddle point, and that all trajectories passing through the dividing surface from the reactant side eventually form products without recrossing the surface.

Conventional TST is almost always combined with the rigid-rotor harmonic oscillator approximation whose failings were discussed in the preceding section. In addition, variational effects and/or tunneling are important in many reactions, and for these systems more accurate dynamical treatments are desirable. Tunneling effects are usually included as a correction, often by a very simple perturbation theory expression derived by Wigner [89]. Though the form of the Wigner factor ensures that the correction is generally a minor one, the approximations made in deriving this correction factor are often of doubtful validity. It is not hard to find cases where tunneling changes the rate constants by more than 1 order of magnitude.

One can very significantly improve the tunneling treatment, as has been repeatedly demonstrated over the past decade, and software for computing various approximate tunneling corrections has also been widely distributed. For example, the Eckart model, which uses the zero-curvature tunneling methodology [4], has been shown to give more accurate estimates of the tunneling than the Wigner formula. Lu et al. [90] have developed a number of more accurate approximations which use additional information about the shape of the PES near a saddle point, notably the various small-curvature tunneling methods.

One can improve TST quite significantly, particularly for cases with loose TS, by selecting a different TS surface for each temperature, or, better, each conserved quantum number (such as E and J); these are called "variational TSTs" (VTSTs) [4, 91, 92, 93, 94]. Over the past 20 years, many VTST calculations have been published, often using the widely distributed VTST codes POLYRATE [90, 95, 96], TheRate [97], and VARIFLEX [98].

About 5 years ago, Miller [3] rewrote the quantum-scattering equations in a way which clarifies their relationship to the TST approximation. A few demonstration calculations [99, 100, 101, 102] have been done using this form of the quantum-scattering equations, which make "exact" rate calculations more feasible than they were previously, but they still appear to be much too expensive for use in engineering applications.

Very recently, several researchers [103] have developed semiclassical methods for approximating the quantum-scattering results; these methods automatically include tunneling effects and recrossing effects at least approximately. There is reason to hope that all these innovations will make much more accurate rate calculations practical sometime in the coming decade.

At present, methods which require accurate energies for more than a few points on the PES are not practical, except for very small systems, because each quantum chemistry calculation requires so much computation time. None of the TST methods just described are sufficiently fast to meet the requirements of existing computerized model-generation codes, where we ordinarily cannot afford to perform even a single quantum chemistry calculation for each reaction. However, several researchers are developing methods for accurately approximating the important regions of the PES without performing many expensive quantum chemistry calculations [104], and it might one day be possible to automate these methods for use in model-generation software.

There is some hope that one may be able to generalize from a very high level calculation on a single system to

derive an improved estimate of the effect of tunneling and recrossing in larger analogous systems; this approach could be quite practical for automated kinetic model construction. For example, Truong et al. [41] recently developed two modified small-curvature tunneling treatments based on a reaction-class approach viz., RC-μV and RC-μi, with the assumption that all reactions in the same class have the same reactive moiety and therefore very similar PESs along the reaction coordinate. These models assume that the effective potential $V_a^G(s)$ and the effective mass $\mu_{eff}(s)$ is essentially invariant across a reaction family, so a careful calculation on one reaction in that family is sufficient for estimating tunneling effects in all the rest.

1.3.4 Methods for treating barrierless reactions

Many important reactions have essentially no barrier in the exothermic direction. This almost completely removes the large uncertainty in ordinary rate constant predictions arising from errors in the calculated or inferred barrier height. The rates of these barrierless reactions are usually only very weakly dependent on temperature. Nonetheless, it remains surprisingly difficult to predict barrierless reaction rate constants quantitatively.

The classical approach to modeling barrierless A + B → C reactions focuses on the long-range attractive potential between A and B. If one or both of the reactants are charged, the strong long-range attraction trumps most other effects, and one can make quite accurate predictions. For neutral molecules, one can as a first approximation use the simplest Gorin algorithm [105], based on locating the TS at the centrifugal barriers [106, 107] for spherically symmetric R^{-6} potentials, i.e., at $r^{\neq} = r_0(6V_0/RT)^{1/2}$, where V_0 is the potential energy of interaction at the minimum bond length, r_0, between the (assumed spherical) molecules. This leads to a simple analytic formula for the high-pressure-limit rate of combination of radicals:

$$k_\infty(T) = 3(2)^{1/6}\Gamma(2/3)\left(\frac{a_A a_B I_A I_B}{I_A + I_B}\right)^{1/2} \times \frac{\pi^{1/2}(k_B T)^{1/6}}{S_{AB}} \frac{M_A M_B}{(M_A + M_B)^{5/2}} ,$$

where a_A and a_B are the polarizabilities of A and B, I_A and I_B are the ionization potentials, M_A and M_B are the masses, and S_{AB} is the symmetry number of the two free radicals. In this model, the internal rotors are considered to be unhindered until a hard-sphere interaction occurs. Note the extremely weak predicted temperature dependence; at high pressures, the experimental temperature dependence is usually very weak and, in practice, one can often neglect the temperature dependence of $k_\infty(T)$ entirely. However, at typical experimental pressures, falloff often gives rise to a measurable temperature dependence in the observed rate.

The real molecular potential is, of course, not spherically symmetric. Also, in the association of neutral radicals, short-range interactions are important and at these separations some of the rotational degrees of freedom become internal rotations, librations, or bending vibrations. As a result, the intermolecular motion is strongly coupled and this leads to breakdown of some of the simplifying assumptions. Benson [2] modified the simple Gorin model by adding a steric factor. In his "restricted free rotor model" at any given separation of active centers, $r^{\neq}$, only certain orientations are allowed, while certain others are not allowed. The statistical adiabatic channel model of Quack and Troe [108, 109] is an alternative to account for the asymmetries in the intermolecular potential and also to include R-dependent variations in the fragment rovibronic energies. For certain classes of reactions, relatively simple rules of thumb based on empirical data allow one to fairly accurately estimate the steric factor required in the Gorin model, or the analogous parameters required in a simplified version of the statistical adiabatic channel model developed by Troe. However, it is difficult to know if these rules of thumb will hold up when predicting the rate of some new types of reaction.

Several variants of VTST have been used successfully to calculate barrierless reaction rates, notably the spectacular agreement between the very detailed experimental data [110] on the microcanonical rate $k(E)$ for singlet-channel ketene dissociation and detailed VTST calculations [111]. However, there are several other cases in the literature where the experimental and theoretical rates for barrierless reactions differ by as much as 1 order of magnitude. It is not always clear whether these discrepancies arise from problems with the experiments (e.g., owing to falloff, see next section), with the rate calculation methodology (different researchers make somewhat different approximations), or with the PESs on which the rate calculations depend.

A significant recent advance is the development and wide distribution of the VARIFLEX software [98] for calculating barrierless reaction rates and correcting for falloff effects, which should allow direct comparison of different methods and greatly accelerate progress in this field.

High-accuracy computation of barrierless reaction rates usually requires a very large number of quantum chemistry calculations to map out a fairly large region of the PES. Therefore, these methods cannot be used directly during automated kinetic model generation. However, one might be able to generalize from a small number of high-accuracy calculations in order to predict a whole family of analogous barrierless reaction rates. To our knowledge, no one has yet tested the accuracy of this sort of generalization.

1.3.5 Pressure-dependent falloff and chemical activation

The methods described in the previous sections (and later in this article) compute the high-pressure-limit rate constant, $k_\infty(T)$. This has the great advantage of putting all the calculations on the same footing and of simplifying the calculations.

However, many gas-phase reactions of technological importance are significantly pressure-dependent, owing to the fact that thermalization rates are slow compared to some reaction steps. This means the activated reaction

intermediates will not have a Boltzmann population distribution, and so cannot be characterized by a temperature. In extreme cases, the behavior can be so strange that the apparent "rate constant" can vary with time [112].

The master equations that describe the pressure dependence have been well understood for many years and are detailed in several textbooks [113, 114, 115]. For many years excellent analyses, software, and approximations have been available for reactions which proceed through a single activated intermediate (a single well on the PES) [113, 114, 115]; however, much less has been done, and much less software is available, for systems which proceed through more than one activated intermediate (multiple wells on the PES). Multiwell [116], the first publicly available computer program which could handle general isomerization networks, was not distributed until 2000.

Most of the methods that have been presented in the literature for computing $k(T,P)$, particularly for multiple-well cases, are rather complex [117] and are not easily automated for use in computerized model-generation software. Many of them are also very computationally intensive. The $k(T,P)$ calculations require a comprehensive listing of all the important reaction and isomerization steps available to each activated intermediate. For polyatomic systems, there are often dozens or hundreds of possible reaction/isomerization pathways. The $k(T,P)$ calculations require estimates of the microcanonical rates, $k(E)$, for each reaction/isomerization step, and estimates of the densities of states, $\rho(E)$, for each intermediate. For highest accuracy, one would perform a detailed rate calculation using the methods described earlier for each reaction/isomerization step, and carefully characterize each reactive intermediate, including its floppy modes, in order to compute the densities of states. Then, one would solve the full master equation to arrive at $k(T,P)$. Unfortunately each of these steps separately would be too computationally intensive for our kinetic-model generator.

Fortunately, some less-expensive approximate methods have been developed. Ritter and co workers [118, 119, 120] have developed a method for rapidly estimating $\rho(E)$ for any species which can be described by a Benson-type thermochemical group, and this method has been automated by Grenda and Bozzelli [121]. The required $k(E)$ can be rapidly estimated from $k_\infty(T)$ using Forst's inverse-Laplace-transform methods [122] or Dean's quantum Rice–Ramsperger–Kassel methods [123]. These methods of computing $\rho(E)$ and $k(E)$ do not require any quantum chemical calculations on large molecules in a homologous series, a tremendous practical advantage over the conventional computationally intensive approach.

Grenda and coworkers [38, 39] have devised a computer algorithm for identifying all the wells and reactions required for a $k(T,P)$ calculation, and Matheu et al. [37] have developed a rigorous screening method for eliminating the insignificant wells and reactions. The solution to the master equations can be dramatically simplified by using Troe's modified strong collision approximation [124]; this approximation is known to be accurate for single-well falloff situations, and it works well for many chemically activated reactions. (Rigorous bounds on the difference between the modified strong collision approximation and the full master equation solution for chemically activated or multiple-well cases have, unfortunately, not yet been established.) Matheu et al. [125] have recently demonstrated that the $k(T,P)$s for several different systems generated by an automated procedure making these approximations are in good agreement with more precise by-hand $k(T,P)$ calculations and are in reasonable agreement with experimental data. On the basis of this recent work, there is reason to believe that if we can accurately and efficiently estimate the $k_\infty(T)$s, it will be possible to automatically calculate suitable $k(T,P)$s inside kinetic-model-generation programs.

1.3.6 Accurate a priori rate constants: summary

Methods for computing reaction rates a priori are now well established, and in many cases it is possible to achieve order-of-magnitude or better agreement with experiment. The expense and difficulty of accurate quantum chemical calculations continues to be the primary limitation, though now the quantum chemistry calculations are often accurate enough that one must be seriously concerned about the approximations made in other parts of the rate calculation, particularly in the treatment of floppy modes, tunneling, and recrossing dynamics. A priori rate calculations are becoming good enough that sometimes it is not clear whether the theoretical or experimental rates are more accurate, and work is required to establish a good set of benchmarks for testing rate calculations. However, a priori rate estimation as currently practiced involves multiple steps, each with its own set of approximations, usually untested. It is quite difficult at present to set reliable uncertainty bounds on a priori rate calculations.

It has recently become feasible to compute the pressure-dependent rate constant $k(T,P)$ for complex chemically activated reactions, presuming that one can accurately compute $k_\infty(T)$ for each step in the chemically activated reaction network. Although further work is required, recent progress suggests that $k(T,P)$ calculations will not be the primary limitation on the accuracy of computer-generated kinetic models.

Although reasonably accurate a priori $k_\infty(T)$ calculations are now possible for at least small-molecule reactions, these calculations are far from being efficient enough to be included in an automated kinetic model builder. At present a single quantum chemical TS calculation might require a week or more of computation time; obviously it would not be practical to compute thousands of rates this way in order to construct a large kinetic model. Instead, much faster methods for estimating $k_\infty(T)$ are required. Classical rate-estimation methods are reviewed in the next section, and modern rate-estimation methods calibrating the fast methods with a limited number of quantum chemical calculations are described and demonstrated further in Sects. 2 and 3.

1.4 A selective review of fast rate-estimation methods

Although the need for large numbers of reaction rate estimates for computer-generated kinetic models is relatively new, chemists and engineers have been making

reaction rate estimates and correlating experimental rate data by rather simple formulae for at least 100 years. Here we selectively review this extensive prior work, which was heavily based on experimental data, as it provides the basis for the quantum-chemistry-based rate-estimation methods we employ.

1.4.1 Definitions and preliminaries

The activation energy, E_{act}, of a chemical reaction is a measure of the temperature dependence of the rate constant, k, of a reaction. In the simple Arrhenius expression, the rate constant is given by

$$k_\infty(T) = A\exp(-E_{act}/k_B T) \ , \tag{2}$$

so the activation energy is defined in terms of the logarithmic derivative of the rate constant:

$$E_{act} = -R\mathrm{d}(\ln k_\infty)/\mathrm{d}(1/T) \ . \tag{3}$$

E_{act} is usually determined experimentally by measuring k over a finite temperature range. Reaction rates do not exactly follow Eq. (2), so E_{act} is not really a constant, but a weak function of the temperature. The conventional TST rate expression is conveniently written

$$k_\infty(T) = \alpha\kappa(T)\left(\frac{N_A k_B T}{h}\right)\frac{Q^{\neq}}{Q^A Q^B}\exp\left(\frac{-E_0}{k_B T}\right) \ , \tag{4}$$

where α is the reaction path degeneracy, $\kappa(T)$ is the Wigner tunneling correction factor corresponding to the magnitude of the imaginary frequency at the activated complex, N_A is Avagadro's number, T is the temperature, and E_0 is the zero-point corrected barrier height. Q^A and Q^B denote the respective total partition functions of the reactants with the zero of energy at the zero-point energy of the motionless reactants. $Q^{\neq}$ is the same partition function of the activated complex with the translational motion along the reaction coordinate being omitted. Note that E_0 is not the same as E_{act}, though often they are similar. Beware that many authors, including Johnston [126], use the classical barrier height, $E_{barrier}$, (no zero-point correction) instead, so their partition functions have different zeroes of energy (and Q_{vib} do not go to 1 as $T \to 0$). As discussed earlier, the TST of reaction kinetics assumes that a chemical reaction between the reactants proceeds via a TS or activated complex and a "quasiequilibrium" is established between the reactants and the activated complex. The conventional TST rate constant k_∞ can then be expressed in terms of a sort of equilibrium constant, $K^{\neq}$,

$$k_\infty = \kappa(T)(k_B T/h)K^{\neq} \ , \tag{5}$$

on the assumption that the quasiequilibrium may be treated as though it were a true equilibrium. By extending the analogy of thermodynamic equilibrium, Eq. (5) can be rewritten as

$$\begin{aligned} k_\infty &= \kappa(T)\frac{V_m k_B T}{h}\exp\left(\frac{-\Delta G^{\neq}}{RT}\right) \\ &= \kappa(T)\frac{V_m k_B T}{h}\exp\left(\frac{\Delta S^{\neq}}{R}\right)\exp\left(\frac{-\Delta H^{\neq}}{RT}\right) \ , \end{aligned} \tag{6}$$

where V_m is the molar volume in the standard state used to define the zeroes of $\Delta H^{\neq}$ and $\Delta S^{\neq}$. For ideal gases $V_m = (RT/P_0)$ and $P_0 = 1$ atm. On taking logarithms of both sides, Eq. (6) shows a linear relationship between $\log k_\infty$ and $\Delta G^{\neq}$. The latter parameter is a kind of free energy of activation, but with one vibrational mode of the activated complex (the reaction coordinate) being discarded.

1.4.2 Linear free-energy relationships

A variety of simple formulae for parameterizing the rate or activation-energy variations between members of the same reaction family have been proposed in the literature. Often these have the form

$$\ln k_i(T) = \ln k_0(T) + m(x_i - x_0) \ , \tag{7}$$

where m is characteristic of the reaction family, x_i is some property (hopefully not too difficult to calculate) of the species involved in the reaction "i", and x_0 corresponds to the reference reaction that defines the family. Perhaps the oldest and most widely used approach is to set $x = \Delta H_{rxn}/RT$, in which case this is called an Evans–Polanyi [127, 128, 129] or Semenov [130] relation, and the proportionality constant, m, is usually denoted by α or γ:

$$E_{act}^i = E_{act}^0 + \gamma\Delta H_i^0 \ . \tag{8}$$

Equation (8), the original form suggested by Evans and Polanyi, is a simplified form of the general Eq. (7), which assumes a constant A factor for the whole reaction family.

Another very popular choice of x is the Hammett [1] σ (for aromatic compounds) or the Taft [131] σ^* (for aliphatic compounds), in which case m is denoted by ρ, an empirical parameter characteristic of a given reaction series.

According to TST (Eq. 5) (neglecting tunneling)

$$\ln k_i(T) = \ln k_0(T) + \left(\Delta G_0^{\neq} - \Delta G_i^{\neq}\right)/RT \tag{9}$$

a linear relation is apparent between the logarithm of the ratio of the rate constants and the difference in the free energy of activation. For reactions with similar free-energy surfaces for reactants and products, it has been suggested [132] that

$$\Delta G_0^{\neq} - \Delta G_1^{\neq} = \beta(\Delta G_0 - \Delta G_1) \ , \tag{10}$$

$$\log(k_2/k_1) = \beta\log(K_2/K_1) \ . \tag{11}$$

This empirical relationship between thermal equilibria and kinetics has been known for many years. All relations of the form of Eq. (7) are sometimes referred to as linear free-energy relationships (LFER), the assumption being that $\Delta G^{\neq}$ is approximately linearly related to quantities such as ΔH_{rxn} or σ or σ^* or ΔG_{rxn}. Often correlations are found to more than one property x, so multilinear forms are also sometimes employed.

1.4.3 Nonlinear formulae for estimating activation energies

The LFER work well because all the reactions in a well-chosen family are very similar, so $(x_i - x_0)$ is usually small and the linear approximation to the true dependence in Eq. (1) does not introduce much error. The actual relationships between the rates and the molecular properties of the species involved are generally nonlinear. For example, by the Hammond postulate, the Evans–Polanyi $\gamma \sim 1$ if $\Delta H_{rxn} \gg 0$, and $\gamma \sim 0$ if $\Delta H_{rxn} \ll 0$, i.e., the slope of the line changes with x!

Several researchers have proposed nonlinear relationships, and most of these are not just fitting formulae but have a strong basis in theory. The most famous of these nonlinear free-energy relationships is the Marcus equation [133, 134, 135] for electron-transfer reactions, which was honored recently with the Nobel prize.

Johnston's bond energy–bond order (BEBO) method [126, 136] for gas-phase hydrogen-abstraction reactions is another nonlinear rate-estimation method which has been widely used for more than 3 decades. The BEBO method is essentially a coupling of TST with empirical relationships that describe the connection between bond energy and bond order. The energy of the reacting bonds was described using Morse curves with the assumption that the order of the bond X....H.....Y is equal to unity all the way along the reaction coordinate from $X + HY$ to the $XH + Y$ state. Activation energies calculated by Johnston et al. and Parr [136] for reactions of X (X = H, Cl, Br, I, R) with HX and RH were in good agreement with experimental data. BEBO was used by Xing et al. [137] and Qui et al. [138] in reactions of OH with haloethanes, Tribert et al. [139] in the reactions of hydrogen atoms with chlorinated and brominated hydrocarbons, and Su et al. [140] in the reaction of $O(^3P)$ with halomethanes to rationalize the reactivity. However, the BEBO method does not work very well for some hydrogen-abstraction reactions involving alkoxyl and peroxyl radicals, with errors of greater than 40 kJmol^{-1} in estimated activation energies [141], prompting the development of new, often more heavily parameterized, formulae which partially capture additional physical effects.

Using Morse potentials of reacting bonds, Zavitsas and coworkers [142, 143, 144] arrived at a simple method of calculating the activation energy of abstraction reactions. E_{act} is expressed as a maximum value of the interaction energy between XH and Y. The interaction energy in turn is defined as the weighted sum of two Morse and anti-Morse curves corresponding, respectively, to the attraction between X and H, U_{XH}, and Y and H, U_{YH}, and the triplet repulsion between X and Y, U_{XY}, in a TS X....H.....Y. The method of Zavitsas and coworkers gives very reasonable estimates of E for reactions with a reaction enthalpy between -60 and $+60$ kJ mol^{-1}.

In the bond strength–bond length method [145], the activation energy was calculated as the difference between the maximal energy of the X.....H.....Y complex ($U_{XH} + U_{YH} + U_{XY}$) and the energy of the YH molecule with the assumption that all along the reaction path of the X + HY reaction, the following condition is conserved:

$$\exp(-2a_i r_i) + \exp(-2a_f r_f) = 1 \quad , \tag{12}$$

where a_i and r_i refer to the Y–H bond and a_f and r_f refer to the X–H bond. This method is conceptually similar to Shustorovich's method [146], which is now used widely for estimating reaction rates on catalytic surfaces.

Other nonlinear formulae for neutral gas-phase reactions (mostly for hydrogen abstractions) include

1. An empirical equation [147, 148] depicting its nonlinear dependence on the dissociation energies of the forming and breaking bonds (D_f and D_i in kilojoules per mole):
$$E_{act} = D_i - 0.0203 D_f (1 + 0.0256 D_i) \quad . \tag{13}$$
The estimates derived from this expression are shown to be in good agreement with experimental values of E_{act} (within $\pm$ 8 kJ mol^{-1});
2. A hyperbolic dependence of E_{act} on the enthalpy of the reaction [149]:
$$E_{act}(E_{act} - \Delta H) = E_{act,0}^2 \quad , \tag{14}$$
where $E_{act,0}$ is the activation energy at $\Delta H = 0$.
3. The curve-crossing model of Denisov et al. [141], which treats the activation energy as the energy difference between the minimum energy of the cleaving bond and the energy corresponding to the point of intersection of the terms characterizing the vibration amplitude of the forming and breaking bonds. This model was further categorized on the basis of whether the forming (Y–H) and breaking (X–H) bonds were expressed as two parabolic or two Morse curves.

The nonlinear formulae often capture the physics of the situation better than the LFER, but they suffer from many important practical problems: one rarely has sufficient data, even for extensively studied reaction types such as hydrogen abstractions, to accurately determine all the parameters, and although the model parameters usually have some physical interpretation, it is usually not possible to calculate these parameters a priori.

1.4.4 Correlations between rates and other molecular properties

Many attempts have also been made to correlate the rate parameters with various properties of the molecules involved, i.e., there are many quantitative structure–property relationships (QSPR) which connect reaction rates and "descriptors" that can be easily computed from the molecular structure. Descriptors can be simple (e.g., the molecular weight, the Hammett σ factors) or rather complex (local hardness, local softness, and the Fukui indices [61, 150, 151]).

There is seldom a clear causal connection between the molecular descriptor and the reaction rate, but these relationships are nonetheless extremely useful for both organic synthesis and reaction engineering.

The ionization energy is one of the measurable molecular properties highly correlated with the rate

coefficients for hydrogen abstraction by the OH radical [152, 153, 154], for addition of $O(^3P)$ [155] and NO_3 [156] across the double or triple bonds in alkenes or alkynes, and for addition of molecular oxygen to alkyl [157] and silyl radicals [158]. Most of the observed correlations can be understood as the variation of the activation energy with quantities related to reactant or product energies. However, for reactions with very little or no activation barrier, this correlation could stem from the variation in the A factor. Paltenghi et al. [159] observed a linear correlation between log k and the radical ionization potential for the almost barrierless reactions of alkyl radicals with ozone. They commented that the variation in the A factor is responsible for the observed correlation. More specifically, Marston et al. [160] found linear plots for log$A$ versus E(HOMO) for the reactions of NO_3 and OH with alkenes.

Krech and coworkers [161, 162] have demonstrated that activation energies for several reactions of the type AB + C → A + BC are highly correlated with the polarizability of AB. In fact, they are related by the empirical equation

$$E_{\mathrm{act}} = F/\alpha_{\mathrm{AB}} \ , \tag{15}$$

where F is an empirical parameter.

Alfassi and Benson [163] have shown correlation between the sum of the electron affinities of the end groups A and C (denoted as I) in the previously mentioned atom-transfer reaction and the activation energies.

For reactions that proceed by a similar mechanism with two different radicals, cross-correlations were often established to predict reaction rates. The reactions of $O(^3P)$ and OH with organic species were successfully correlated by Atkinson [153, 164] and by Gaffney and Levine [152], while those of NO_3, OH, and $O(^3P)$ reactions were correlated by Atkinson [164], Sablijic and Güsten [165], Grosjean and Williams [166], and Canosa-Mas et al. [167].

The intrinsic barrier for radical additions to multiple bonds is sensitive to the polarizing ability of the π bond and consequently to the electronic nature of the substituents attached to the multiple bond. Various forms of structure–activity relationships have been proposed for use in the kinetics of addition reactions. The rate constant of any substituted system can be estimated according to

$$k_i = k_0 \prod_{i=1}^{n} f(X_i) \ , \tag{16}$$

where k_0 is the rate constant for the reference (unsubstituted) reaction and $f(X_i)$s are the group factors for the substituents. Group factors have been derived for radical addition to alkenes [168], for the reactions of OH with halocarbons [169, 170, 171, 172] and for the reactions of NO_3 [168]. The drawback of this method is that it requires a large database of kinetic data to derive the group factors.

Bakken and Jurs [173] used multiple linear regression and computational neural networks to develop QSPRs for methyl radical addition rate constants. Structure-based descriptors, which can be categorized as topological, geometric, electronic, or hybrid, were defined to encode the substrate information. Descriptors identified during linear model formation were used to build a three-layer, fully connected, feed-forward computational neural network. The major drawback of this compounded nonlinear fitting procedure is its requirement of a large set of experimental data; this is particularly difficult for the addition reactions, since it is usually necessary to correct the experimental measurements for pressure dependence and for competing side reactions (e.g., hydrogen shifts to form resonantly stabilized radicals). There are several difficulties with all QSPR approaches, notably that many of the molecular descriptors are correlated with each other, so the QSPR relationships derived are usually not unique nor are they guaranteed to reflect any physical relationship between the structure and the correlated property.

Correlations between reaction rates and properties derived from quantum chemical (or semiempirical) calculations on the reactant molecules were identified by Blowers and coworkers. Such correlated properties include the bond distortion energy [174], the curve-crossing energy [175, 176], Pauli repulsion energies [177], and so forth.

Klamt [178, 179] devised a series of reactive indices called local frontier orbital descriptors, viz., charge-limited effective HOMO energy, energy-weighted effective HOMO energy, and energy-limited effective frontier orbital charges. These are partly local and partly derived from frontier orbital theory. Klamt's calculations, similar to others in the literature, are based on relatively fast semiempirical AM1 calculations. He arrived at a new molecular-orbital based method called MOOH for estimating the rate constants of degradation of organic compounds by hydroxyl radical viz., the addition of OH to carbon double bonds, the addition of OH to aromatic rings, and hydrogen abstraction by OH from aliphatic carbon atoms, ketones, aldehydes, alcohols, ethers, carbonic acids, and alkynes.

Although there clearly is an empirical correlation between the measured rate parameters and the orbital energies of the reactants, it is not completely clear to these authors that the correlation is causal, as the orbital energies themselves are highly correlated with many other molecular properties. (This is a general problem with using correlation where the underlying physics behind the correlation is unclear.)

1.4.5 Semiexperimental reaction rates – TK

Most rate data are measured over a very restricted range of temperature and pressure, owing to experimental limitations. While it is clear that there is no ultimate substitute for experimental $k(T,P)$ measurements, Benson and coworkers [2, 180] developed the TK formulation of conventional TST to extrapolate the rate coefficients to temperature regimes outside the range of experimental data. This method is of wide use in predicting kinetic information for cases where there are few data available, and for roughly estimating reaction rates where no data are available. In the TK-TST method, thermochemical properties of stable molecules

are determined using experimentally based group-additivity (GA) methods [181], while TS properties are estimated using statistical mechanics by comparing assumed TS structures with known structures of stable molecules. Model calculations of well-established rate constants calibrated the guesses about the transition structure. (At the time Benson developed TK-TST it was not possible to calculate accurate TS structures by ab initio methods). The method has been tested carefully in a few cases where a large number of data are available: see, for example, Cohen's [182, 183, 184] work on the metathesis reactions of H, O(^{3}P), and OH with a series of alkanes. On the basis of a similar idea, Ranzi et al. [185] arrived at empirical rate rules for abstraction reaction families through a critical evaluation of the experimental data.

The finding by Benson and coworkers that both molecular and TS thermochemical properties can be represented as a sum of component-group properties provides the basis for the generalization of molecular classes and reaction families discussed at length in this article. Our protocol to arrive at generic rate rules is similar to the TK-TST method, except for the fact that we aim to efficiently utilize the wealth of quantum chemical information on TS structures and properties that is now becoming available with modern computers and the computational approaches described in Sect. 1.3.

1.5 Generalization from a priori reaction rates

Virtually all the fast rate-estimation methods in the literature are based on experimental rate measurements, and so are limited to reaction families where good reaction rate data are available. A priori rate calculations are now accurate enough that they can be used as the source data, with the advantages that a very large amount of detailed data is available from a single quantum chemical calculation, and calculations can be performed on systems that are not experimentally convenient.

1.5.1 Reaction-class TST

Truong [42] developed the reaction-class TST to predict the thermal rate constant of any member of a reaction in a given class from that of the principal reaction using two energetic properties, namely, the differential barrier height and the reaction energy. It is based on the TST framework with the concept that all elementary reactions in a given class have the same reactive moiety and consequently very similar PESs along the reaction coordinate. With this notion they factored the ratio of the rate constants, k_2/k_1, into different components, namely, tunneling, reaction symmetry, partition functions, and potential energy. The factors from tunneling and partition functions were taken to be unity, thus avoiding the need to perform frequency calculation for large molecules in the reaction class; however, for every new member of the class, additional energy calculations at high levels of theory are needed to predict the reaction rate. Though reaction-class TST saves computer time, it still requires a quantum chemical TS calculation for each reaction, and so is not practical for computer generation of kinetic models.

1.5.2 GA for TSs

To this end, we came up with the idea of forming new thermochemical groups (supergroups) corresponding to the reactive moiety in the transition structures of a given reaction class. Such supergroups together with existing thermochemical groups for stable moieties would enable the modelers to derive the free energy of activation of any reaction in a given class at any given temperature and therefrom its reaction rate. In contrast to the GA values (GAVs) of Benson, which are derived semiexperimentally, we derive our TS-specific groups from quantum chemical calculations. As inherent in the second-order GA approximation, this treatment assumes that the total molecular property is the sum of its group contributions and does not account for non-next-neighbor effects. Secondly, while deriving the supergroups we partition the thermochemical properties of transition structures using conventional GA contributions for the unreactive moiety. This assumes that quantum chemical calculations are accurate enough to reproduce the GAVs for stable molecules.

In our first article [186], we developed a systematic procedure for the accurate calculation of thermochemical properties from quantum chemically derived molecular parameters and tested its performance on alkanes and alkyl radicals. We arrived at ways of partitioning the thermochemical properties of transition structures into contributions from reactive and unreactive moieties using GA tables. We demonstrated the near constancy of the thermochemical values of the reactive moiety among the members of the following reaction classes:

$$R\mathrm{CH_3} + Y \rightarrow R\mathrm{CH_2} + Y\mathrm{H};$$

$$(R = \mathrm{CH_3}, \mathrm{Et}, \mathrm{Pr}, \mathrm{Bu}, i\text{-PR}, t\text{-Bu}, sec\text{-Bu}, i\text{-Bu}) \ ,$$

$$RR'\mathrm{CH_2} + Y \rightarrow RR'\mathrm{CH} + \mathrm{H}Y$$

$$(R = \mathrm{CH_3}, \ \mathrm{Et}, \mathrm{Pr}, i\text{-Pr}; R' = \mathrm{CH_3}) \ ,$$

$$R_2\mathrm{C}R'\mathrm{H} + Y \rightarrow R_2\mathrm{C}R' + Y\mathrm{H}(R = \mathrm{CH_3}; R' = \mathrm{CH_3}, \mathrm{Et}) \ ,$$

with $Y = \mathrm{H}$ and $\mathrm{CH_3}$. The average of its contribution in a given class is identified as the supergroup value for the reactive moiety (see Sects. 2.3, 2.4 for details). We also showed that the same supergroup contribution is obtained in the previously mentioned classes of reaction by considering the reaction in either direction. We demonstrated the usefulness of this observation for establishing the thermochemical values of radicals with large experimental uncertainty. We compared the rate predictions based on our supergroup GA procedure with experimental data and literature rate estimates and discussed the levels of accuracy achievable by this procedure. Since supergroups per se are not Benson groups, we developed protocols for splitting the supergroups into Benson groups using the thermochemical properties of symmetric transition structures associated

with the reactions $CH_3CH_2 + CH_3CH_3$, $(CH_3)_2CH_2 + (CH_3)_2CH$, $(CH_3)_3CH + (CH_3)_3C$, $H + H_2$, and $CH_3 + CH_4$. We developed ten new groups covering all probable intermolecular abstractions by alkyl groups from alkanes and four new groups corresponding to abstraction by hydrogen atoms from alkanes.

Subsequently [187] we extended the treatment to hydrogen abstraction from alkenes, alkynes, alcohols, aldehydes, and acids by hydrogen atoms and developed 16 new groups for rate predictions. With polar substrates such as alcohols, aldehydes, and acids, we observed a systematic but small variation in the enthalpy value of the supergroup across the members of the given reaction class. Subsequently, we investigated the non-next-neighbor effects [188] on supergroups by including more members with β substituents of extreme electronic and steric nature, viz., $CH_3CH_2X + Y \rightarrow CH_2CH_2X + YH$ [X = F, Cl, Br, OH, SH, NH_2, OCH_3, OC(O)H, $OC(O)CH_3$, CHO, $COCH_3$, COOH, $COOCH_3$, etc.]. We proposed means of accommodating [188] non-next-neighbor effects on reaction rates using a multilinear expression based on the electronic, σ, steric, R_s, and hyperconjugative (HC) parameters of the substituent, namely, $\Delta H^{298}(X) = \Delta H^{298}(R\text{–H}) + a_1{*}\sigma(X) + a_2{*}R_s(X) + a_3{*}\text{HC}(X)$. We also derived a qualitative rationale through atoms-in-molecule analysis for the partitioning of energy obtained from quantum chemical calculations using GA.

2 Computational methodology

2.1 Ab initio calculations

Standard ab initio molecular orbital theory calculations were carried out with the GAUSSIAN 98 suite [189] of programs. The geometry of the reactants, TSs, and products of the reactions considered in the present study were optimized at the (U)MP2(FC)/6-31G(d′) level. The energies were calculated using the CBS method, CBS-Q of Ochterski et al. [51, 52] which combines the extrapolated CBS second-order limit with higher-order correlation [MP3, MP4, QCISD(T)] energies derived at a relatively smaller basis set for the accurate calculation of molecular energies. The method also includes an empirical correction and a correction for spin contamination in order to achieve improved agreement with experimental data. The ab initio heats of formation of molecules at 298.15 K were obtained from the calculated heat of atomization at 0 K and the experimental heat of formation of atoms using the commonly adopted procedure [190]. The atomization energy was further corrected [191] for spin–orbit interaction from the energies of the atoms and isodesmic bond additivity corrections. Besides this single-point high-level energy calculation at a TS geometry obtained at MP2(FC)/6-31G(d′), we also searched the intrinsic reaction coordinate, IRC(MP2(FC)/6-31G(d′), and did IRC-MAX[74] calculations, Max{CBS-Q}//IRC{MP2(FC)/6-31G(d′)}, to obtain the upper bound for the classical barrier heights. The IRC was determined by following the reaction path with a stepsize of 0.1 bohr (0.0529 Å).

Furthermore, some of the prototypical transition structures were also optimized at G2 and B3LYP levels for the purpose of comparison. Both the compound CBS-Q and G2 methods are expected to have nearly the same optimized geometry as optimizations are done, respectively, at MP2(FC)/6-31G(d′) and MP2(FU)/6-31G(d) levels. The former basis is a modified version of the latter and is obtained by combining the 6-31G sp functions with the 6-311G** polarization components. B3LYP optimizations were done, however, with relatively larger basis sets namely, CBSB3 and CBSB7. The latter geometry is used in CBS-QB3 and Max{CBSQB3}//IRC{B3LYP/CBSB7} model chemistry calculations.

2.2 Calculation of thermochemical properties

The total partition function, Q_{tot}, of all species was calculated within the framework of the rigid-rotor-harmonic-oscillator approximation with corrections for internal rotation. The MP2/6-31G(d′) optimized geometrical parameters and the scaled (0.91844) harmonic vibrational frequencies computed at the HF/6-31G(d′) level were used for the calculation of rotational and vibrational partition functions. All torsional motions about the single bonds between polyvalent atoms were treated as hindered internal rotations. The hindrance potential for the internal rotation was obtained at the HF/6-31G(d′) level by optimizing the $3N-7$ internal coordinates, except for the specific dihedral angle which characterizes the torsional motion. This dihedral angle was varied from 0° to 360° in increments of 20° or 30°. The PES thus obtained was then fitted to a Fourier series $\Sigma_m A_m \cos(m\phi) + B_m \sin(m\phi)$, with $m \leq 17$. Subsequently, the partition function for the hindered rotation was obtained by solving the Schrödinger equation

$$-\frac{h^2}{8\pi^2 I_{hir}}\frac{d^2\Psi(\Phi)}{d\Phi^2} + V(\Phi)\Psi(\Phi) = E(\Phi)\Psi(\Phi) \tag{17}$$

for the energy eigenvalues with the fitted hindrance potential using the free rotor basis function. The reduced moment of inertia for rotation, I_{hir}, in the kinetic energy term was taken as the reduced moment of the two groups about an axis passing through the center of gravity of both the groups. Though I_{hir} is actually a function of ϕ and the vibrational coordinates, in the present work I_{hir} was fixed at its value for the equilibrium geometry, and the rotating group was assumed to be rigid. The partition function for hindered rotation was evaluated by direct counting, while the thermodynamic properties H, S, and C_p were calculated from the ensemble energy averages and fluctuations in internal energy, respectively, $< E >^2$ and $< E^2 >$.

2.3 Derivation of supergroup values from the thermochemical properties of TS

The procedure to derive GAVs for the constant reactive moiety (supergroup) from the thermochemical properties of TSs essentially stems from the assumptions that the thermochemical contribution from the unreactive moiety in the TS is nearly the same as in the reactant and that it is equal to that of Benson's group values. Consequently, the GAVs for reactive centers were derived by balancing the ab initio calculated $\Delta H^{\neq}$(298.15 K), $\Delta S^{\neq}$(298.15 K), and $\Delta C_p^{\neq}(T)$ for the difference between reactants and TSs with those derived from Benson's GA table. For example, the theoretically calculated $\Delta H^{\neq}$ at 298 K for $C_2H_6 + HO_2 \rightleftharpoons CH_3CH_2 - H - O_2H$ is given by

$$\Delta H^{\neq}(\text{calc}) = E_0 + \Delta H^{0\rightarrow 298}(\text{TS}) - \Delta H^{0\rightarrow 298}(C_2H_6) - \Delta H^{0\rightarrow 298}(HO_2)\,, \tag{18}$$

where $\Delta H^{0\rightarrow 298}$ denotes the thermal contribution to the enthalpy at 298.15 K and E_0 is the energy difference between the reactants and the TS at 0 K. The ab initio $\Delta H^{\neq}$ value is then equated to the GA expression:

$$\begin{aligned}\Delta H^{\neq} &= \text{GA(TS)} - \text{GA}(C_2H_6) - GA(HO_2)\\ &= H\{C/C/H3\} + H\{C/C/H2/-H/O/O\} + H\{O/O/H\}\\ &\quad - 2H\{C/C/H3\} - H\{HO2\}\ .\end{aligned} \tag{19}$$

The notations H{C/C/H3} and H{O/O/H} correspond to Benson's heat of formation group values for $-CH_3$ and $-O_2H$ moieties, and H{HO2} represents the heat of formation for the HO_2 radical. Finally, the supergroup value H{C/C/H2/−H/O/O} signifies the enthalpy associated with the reaction center or the reactive moiety CH_2–H–O in the TS. The migrating hydrogen in the reactive moiety is represented as −H in our definition of the reactive moiety. Since {C/C/H2/−H/O/O} contains three polyvalent atoms, it is not a group per se in the sense of Benson's definition;

hence we refer to it as a supergroup. Taking both expressions for $\Delta H^{\neq}$ together, we obtain ΔH^{298} for this supergroup:

$$H\{C/C/H2/-H/O/O\} = \Delta H^{\neq}(\text{ab initio}) - H\{O/O/H\} + H\{C/C/H3\} + H\{HO2\} \quad . \tag{20}$$

Similar to bond dissociation energies (BDE), we only need the difference between the calculated TS and reactant energies in order to estimate the heat of formation value of the reactive moiety (supergroup). Analogous formulae allow one to determine the intrinsic entropy and temperature-dependent heat capacity, $C_p(T)$, group values for the reactive moiety. However, to determine the intrinsic entropy, $S_{int} = S + R\ln(\sigma/n_i g_e)$, of supergroups, a quantity devised by Benson to account for the symmetry, σ, electronic degeneracy, g_e, and optical isomers, n_i, of the system, one should take into account the symmetry of the reactants and TS through the following expression:

$$S_{int}\{C/C/H2/-H/O/O\} = \Delta S^{\neq} + S\{C/C/H3\} + S\{HO2\} - S\{O/O/H\} - R\ln\left(\frac{\sigma_{HO_2}\sigma_{C_2H_6}n_{TS}}{\sigma_{TS}n_{HO_2}n_{C_2H_6}}\right) \quad . \tag{21}$$

2.4 Generic rate estimation from supergroup and Benson's group values

The generic rate constant for attack on a primary alkyl C–H bond by HO_2,

$$RCH_2CH_3 + HO_2 \rightarrow RCH_2CH_2 + H_2O_2 \quad ,$$

can then be calculated from the {C/C/H2/−H/O/O}, {C/C/H3}, {HO2}, and {O/O/H} group values using the conventional TST expression (Eq. 6). The free-energy change associated with this class of reactions, $\Delta G^{\neq}(T) = \Delta H^{\neq}(T) - T\Delta S^{\neq}(T)$, equals the difference between the sum of the free energies of the {C/C/H2/−H/O/O}and {O/O/H} groups and that of the {C/C/H3} and {HO2} groups. The heat capacity values of each of these groups were fitted to a fourth-order polynomial in T and subsequently its analytical integrals were used in conjunction with S^{298} and H_f^{298} values, respectively, to obtain $H(T)$ and $S(T)$. The $\Delta G^{\neq}(T)$ and therefrom the per hydrogen abstraction rate were then calculated from $H(T)$ and $S(T)$. The total abstraction rate for each molecule was obtained by multiplying the per hydrogen rate with the reaction path degeneracy factor.

2.5 Calculation of the tunneling correction factor, $\kappa(T)$

The rate calculated using the supergroup values does not include the tunneling contributions at low temperatures. To account for quantum mechanical tunneling effects, we calculated the transmission coefficients, $\kappa(T)$, using the simple Wigner [89] perturbation theory formula:

$$\kappa(T) = 1 + \frac{1}{24}\left(1.44\frac{\nu_i}{T}\right)^2 \quad , \tag{22}$$

where ν_i is the magnitude of the imaginary frequency in reciprocal centimeters corresponding to the reaction coordinate at the TS and T is the temperature in Kelvin. Since the magnitude of the imaginary frequency and the barrier height remains nearly the same for all reactions in a given class, instead of the simple Wigner tunneling correction one can also calculate the tunneling correction for the first member of the reaction series using any of the improved semiclassical theories and assume the same $\kappa(T)$ for all other reactions in the class.

2.5 Splitting supergroups into Benson groups

The supergroups introduced in our work are very large and do not follow Benson's definition of a group. Permutation of individual polyvalent atoms in such supergroups will evidently lead to a large number of different supergroups making the methodology less useful. Therefore, we arrived at a protocol to further subdivide the supergroups into smaller fractions or groups in the spirit of Benson. We took each polyvalent atom in the reactive moiety as the center of a new group. To make this partitioning scheme unique, we defined the thermochemical group values {−H/*X*2} in symmetric TSs to be zero. With this assumption we derived the group values for the hydrogen loss, viz., {H/−H}, {O/O/-H}, {C/H3/−H}, {C/C/H2/−H}, {C/C3/−H} and {C/O/H2/−H}, respectively, from the thermochemical properties of symmetric TSs, viz.,

$$H\text{–}H\text{–}H = 2\{H/-H\};$$
(by equating the central $\{-H/H_2\} = 0$) ,

$$HO_2\text{–}H\text{–}O_2H = 2\{O/O/H\} + 2\{O/O/-H\} \text{(by setting } \{-H/O^p2\} = 0) \quad ,$$

$$H_3C\text{–}H\text{–}CH_3 = 2\{C/H3/-H\}; \text{(by equating the central } \{-H/C^{me}2\} = 0) \quad ,$$

$$CH_3CH_2\text{–}H\text{–}CH_2CH_3 = 2\{C/C/H2/-H\} + 2\{C/C/H3\};$$
(by equating the central $\{-H/C^P2\} = 0$) ,

$$(CH_3)_3C\text{—}H\text{—}C(CH_3)_3 = 2\{C/C3/-H\} + 6\{C/C/H3\};$$
(by equating the central $\{-H/C^t2\} = 0$) .

Substitution of these group values in the asymmetric TSs provided a means of estimating the central asymmetric group {−H/*X*/*Y*}. The whole procedure is based on the idea that the group value {−H/*X*/*Y*} is a measure of asymmetry in the forming and breaking bonds of a TS. In the present work, we use the symmetric TS HO2–H–O2H to obtain the group value {O/O/−H}. This in combination with the supergroup {C/C/H2/−H/O/O} and {C/C/H2/−H} yielded the TS-specific group {−H/C/O^P} where O^P stands for peroxy oxygen atom. The whole procedure involves redistribution of the thermochemical values of the reactive moiety into three TS-specific groups and does not involve any averaging or fitting procedure.

3 Results and discussion

3.1 Overview

Here we demonstrate our TS GA rate-estimation method by applying it to six reaction families:

$$CH_4 + HO_2 \rightarrow CH_3 + H_2O_2 \quad ,$$

$$RCH_3 + HO_2 \rightarrow RCH_2 + H_2O_2 \quad (R = CH_3,\ \text{Et},\ \text{Pr},\ i\text{-Pr},\ \text{Bu}, t\text{-Bu}) \quad ,$$

$$R_2CR'H + HO_2 \rightarrow R_2CR' + H_2O_2 (R = CH_3, R' = CH_3, \text{Et}) \quad ,$$

$$CH_4 + O \rightarrow CH_3 + OH \quad ,$$

$$RCH_3 + O \rightarrow RCH_2 + OH (R = CH_3, \text{Et}, \text{Pr}, i\text{-Pr}, t\text{-Bu}) \quad ,$$

$$CH_3OX + H \rightarrow CH_2OX + H_2$$
$$[X = H, CH_3, \text{Et}, i\text{-Pr}, t\text{-Bu}, C(O)H, C(O)CH_3, OH, OMe] \quad .$$

We demonstrate that we can accurately compute the thermochemistry for all the stable species in Sect. 3.2. Quantum chemistry methods have considerably more trouble with the TSs of reactions involving O–H bond-forming; we discuss these problems in detail and attempt to resolve some controversies in the literature in Sect. 3.3. In Sect. 3.4. the best quantum chemistry calculations are used to derive TS-GA rate-estimation rules, to check how transferable the group values we obtain are, and to compare the rate estimates in Sect. 3.5 with the limited available experimental data.

Our supergroups for hydrogen abstraction are defined considering only the nearest neighbors of the abstracting origin and the terminus, in line with Benson's group definitions; however, it is not clear whether supergroup values defined this way will be transferable with extremely different β substitutents. Our earlier study gave examples where this substituent effect was rather large. If we expanded the size of the supergroup encompassing the β substituents, a huge number of calculations would be required to fill out a complete table of supergroup values for important reactions and one would lose the advantage of generalization. In those cases, we prefer to seek a linear relationship based on easily computed properties of the substituents [188].

In the present case, it is clear that the isolated oxygen atom O(^{3}P) is very different chemically from the terminal oxygen atom in HO_2, so these two oxygens will require different supergroups and different notation. However, one might hope that the hydrogen-abstraction reactions are rather insensitive to the exact identity of the *R* groups in the alkane part, so it would be reasonable to look for supergroups such as {C/C/H2/−H/O/O} and {C/C/H2/−H/O(^{3}P)}. We test how transferable these group values are in Sect. 3.4. In contrast to our earlier work [186] on thermoneutral reactions with synchronous bond formation and bond breaking, herein, we try to investigate highly endothermic reactions which, as per Hammond's postulate, are expected to proceed through late and asynchronous TSs. As shown in Sect. 3.2, the bond strengths, $D(XOCH_2{-}H)$, are sensitive to the substitutent *X*, so we expect that the rate of hydrogen-atom attack on these CH bonds will also depend on *X*. However, instead of attempting to derive supergroup values for every possible substituent *X*, we will try to find an LFER which will handle the *X* dependence, so we can group these reactions into a single reaction family which we will call {C/H2/O/−H/H}. All of these analyses in Sect. 3.4 assume we can accurately calculate at least a few of these reactions using quantum chemistry; these quantum chemical calculations are discussed in some detail in Sects. 3.2 and 3.3.

3.2 Thermochemical predictions for stable molecules

The performance of CBS-Q level of calculations in reproducing the experimental thermochemical properties of alkanes, C_nH_{2n+2} ($n = 1{-}5$), was demonstrated in the first article [186] of this series, while that of alcohols and esters was shown in the successive articles [187, 188] of this series. We compare our ab initio results at the CBS-Q, CBS-QB3, and G2 levels for the HO_2, H_2O_2, and CH_3OOH systems along with GA and experimental values tabulated in the NIST webbook in Table 1. The ΔH_f^{298} of the reactant radical, HO_2, exhibits a large deviation between the NIST and GA estimates. Benson originally suggested a value of 5 kcal mol^{-1}, while the currently accepted value [192] is 3.5 kcal mol^{-1} following the experimental work of Howard [193]. A bond energy (ΔH^{298}) of 88.2 kcal mol^{-1} was then obtained for ΔH^{298}(HOO−H). This bond energy is then assumed to be equal to the generic *R*OO−H bond energy of alkyl hydroperoxides. Since there are more experimental data on enthalpies of alkyl peroxy radicals than alkyl hydroperoxides, $\Delta H_f^{298}(ROO)$ is often used with $\Delta H^{298}(HOO{-}H) = 88.2$ kcal mol^{-1} to estimate ΔH_f^{298}(*R*OOH). Kondo and Benson [194] performed a measurement for $\Delta H^{298}(CH_3OO) = 5.5 \pm 1.0$ kcal mol^{-1}. This together with *R*OO−*H* BDE and $\Delta H^{298}(H) = 52.1$ kcal mol^{-1} provided the estimation of $\Delta H^{298}(CH_3OOH) = -30.6$ kcal mol^{-1}. On the basis of G2 calculations, Lay and Bozzelli [195], however, recommended a new enthalpy group value of −5.5 kcal mol^{-1} as compared to Benson's value of −4.5 kcal mol^{-1} for the {O/C/O} group. As can be seen from Table 1, the CBS-Q estimate for CH_3OOH is in good agreement with Benson's GA prediction (−30.9 kcal mol^{-1}), while the G2 and CBS-QB3 estimates are in good agreement with Bozzelli's recommendations (−31.9 kcal mol^{-1}).

The structure of the hydroperoxyl radical is dictated by that of O_2. The O−O bond length in the lowest $^2A''$ ground state of HO_2 is 1.3291 Å, while that of the first excited state ($^2A'$, $\Delta E = 0.871$ eV) is 1.3933 Å. All

Table 1. Comparison of calculated thermodynamic properties of peroxy compounds with group additivity predictions and experimental data. ΔH_f^{298} is given in kcal mol^{-1}, S^{298} and $Cp(T)$ data are in cal mol^{-1} K^{-1}. *NIST* = NIST webbook: http://webbook.nist.gov. (HO) implies harmonic oscillator treatment for the O–O torsional mode in peroxides

Species	Method/source	ΔH_f^{298}	S^{298}	C_p^{300}	C_p^{400}	C_p^{500}	C_p^{600}	C_p^{800}	$C_p^{1,000}$	$C_p^{1,500}$
HO_2	CBS-Q	3.59	54.51	8.26	8.76	9.30	9.79	10.57	11.17	12.18
	G2	3.80	54.58	8.31	8.85	9.40	9.90	10.68	11.27	12.26
	CBS-QB3	2.47	54.68	8.30	8.83	9.39	9.89	10.68	11.27	12.26
	GA[a,b]	3.50	54.40	8.34	8.95	9.48	9.96	10.76	11.39	12.45
	NIST	0.50	54.75	8.34	8.95	9.48	9.96	10.76	11.39	12.45
H_2O_2	CBS-Q(HO)	−32.24	55.59	10.07	10.98	11.87	12.65	13.89	14.86	16.61
	G2(HO)	−31.88	55.57	10.10	11.07	11.99	12.78	14.03	15.00	16.74
	CBS-QB3(HO)	−33.18	55.88	10.26	11.27	12.18	12.95	14.13	15.05	16.72
	GA[a]	−32.60	55.70	10.40	11.60	12.60	13.40	14.40	15.00	16.40
	NIST	−32.53	55.68	10.33	11.63	12.55	13.27	14.32	15.05	16.35
CH_3OOH	CBS-Q(HO)	−30.75	66.12	14.73	17.15	19.44	21.44	24.64	27.06	30.95
	G2(HO)	−31.71	66.04	14.87	17.38	19.71	21.73	24.93	27.34	31.18
	CBS-QB3(HO)	−31.89	66.76	15.10	17.63	19.93	21.89	24.97	27.30	31.06
	GA[a]	−30.88	66.85	15.09	17.34	19.40	21.19	24.42	26.47	30.58
	NIST	−31.31		15.03	17.60	20.02	22.13	25.50	28.03	32.02

[a] From Benson's thermochemical kinetics [2]
[b] ΔH_f^{298} from Ref. [192]

peroxide systems are highly correlated systems owing to the presence of lone pairs of electrons on adjacent oxygen atoms. Consequently, the description of the O–O bond length and force constants is very sensitive to the level of theoretical treatment. The compound quantum chemistry methods employed in this study account for correlation corrections to total molecular energy; however, correlation is ignored when computing the Hessian matrix. The latter is being done only at an uncorrelated HF level with a smaller basis set, namely, at HF/6-31G(d′) and HF/6-31G(d), respectively, in the CBS-Q and G2 methods. In this regard, frequencies computed at the B3LYP level with a triple-zeta CBSB7 basis set (in CBS-QB3) are expected to include correlation effects. The calculated O–O stretching frequency in H_2O_2 is around 943 cm^{-1} at the B3LYP/CBSB7 level, while at the HF/6-31G(d′) level the corresponding vibration has been shifted to 1,150 cm^{-1}. Also, the O–O torsional vibration lies at 398 and 343 cm^{-1}, respectively, at the CBS-QB3 and G2 levels. Consequently, the $C_p(T)$ at low temperatures differ by approximately 0.3 cal $mol^{-1}K^{-1}$ between the CBS-QB3 and the CBS-Q and G2 methods. The calculated rotational barrier about the O–O bond is around 9.8 kcal mol^{-1} at both levels. As can be seen from Table 1, the agreement of the S^{298} and $C_p(T)$ values at temperatures less than 1,000 K between the experimental and the CBS-QB3 method is better than with the HF-based frequencies. Since the O–H and O–*R* bonds are nearly at right angles to each other in hydroperoxides, they exist in right- and left-handed forms. Consequently, the symmetry correction depends upon the choice of the statistical treatment between a vibration or a hindered rotation for the torsional motion around the O–O bond. When treated as a harmonic vibration, the entropy value should be incremented by *R*ln2.

3.3 Quantum chemistry calculations of the TSs

The predictive ability of quantum chemistry methods towards the thermochemical properties of TS structures cannot be determined purely on the basis of the thermochemistry of stable molecules. One seldom has sufficient experimental rate data to determine conclusively if a TS calculation is correct; in practice the best one can usually do is to compare several different types of calculations to see if they are consistent with each other and converge towards the same value. If they are consistent, it is usually safe to assume they are at least semiquantitatively correct; if there are significant discrepancies, higher-level calculations may be required.

For the reactions of HO_2 and $O(^3P)$, prior reports suggest that rather high-level calculations may be required. It is known that the B3LYP method can encounter serious difficulties [196, 197, 198, 199] in constructing the minimum-energy reaction path of even simple hydrogen-transfer processes [200] such as $OH + H_2 \rightarrow H_2O + H$ and in predicting the behavior of the hydrogen atom in its addition and elimination reactions [201], either in radicals and radical cations or in triplet states. Either no transition structures can be found at all or when a transition structure is actually located, serious discrepancies are often found in both the geometries and energies, compared to high-level molecular orbital calculations or experiment. Consequently, we perform calculations at different levels, viz., CBS-Q, CBS-QB3, G2, B3LYP/CBSB3, CBS-QB3//IRCMAX, for the prototypical reactions from the HO_2 abstraction reaction families.

Abstraction by HO_2 from alkanes is highly endothermic (approximately 9.2–16.5 kcal mol^{-1}) (Table 2). Consequently, in accord with Hammond's postulate, these reactions are characterized by late TSs with bond formation being advanced over bond cleavage. The MP2/6-31G(d′) optimized geometries, vibrational frequencies, and moments of inertia of 25 transition structures studied in the present work are given in the supporting information. The characteristic geometrical parameters of the reactive moieties, i.e., the bond lengths of the breaking C–H and forming O–H bonds and the associated bond angles are tabulated in Table 3. The geometry of the reactive moiety remains nearly the same at a chosen level of theory and agrees in most cases up to the second decimal value throughout the test set of reactions in each family. This former observation supports the hypothesis that the reactive moiety is not strongly affected by changes to the nonreactive moiety, and suggests the supergroup value will be transferable. (The important exception is the substituent-sensitive reaction family $CH_3OX + H \rightarrow CH_2OX + H_2$, where a single supergroup value is not transferable, as discussed in the following.)

3.3.1 Detailed discussion of the TS geometry for HO_2 reactions

It is interesting to compare the optimized geometries obtained at the B3LYP and MP2 levels for the simple prototypical reactions ($CH_4 + HO_2$, $CH_3CH_3 + HO_2$, $(CH_3)_2CHCH_3 + HO_2$, and $(CH_3)_3CH + HO_2$) tabulated in Table 4. (MP2 geometries are used in the CBS-Q and G2 composite methods.) B3LYP predicts a relatively long C–H distance (longer by about 0.1Å) and also a well-progressed forming O–H bond, (shorter by about 0.05Å) compared to MP2. Interestingly, increasing the size of the basis set from CBSB7 to CBSB3 at the B3LYP level alters the geometry in the direction of the CBS-Q predictions and places the optimized geometry between the CBS-Q and CBS-QB3 extremes (CBS-Q; B3LYP/CBSB3; CBS-QB3). Furthermore, results of the Max{CBS-QB3}//IRC{B3LYP/CBSB7} calculations (Table 5) on $CH_4 + HO_2$, $CH_3CH_3 + HO_2$, and $(CH_3)_3CH + HO_2$ systems using the IRCs reveal the geometry corresponding to the upper bound for the barrier height to be much closer to that of the MP2 result. We also performed additional IRCMAX calculations (Max{CBS-Q}//IRC{MP2/6-31G(d′)}) to obtain the upper bounds for barrier heights and approximate geometries of the TS. Both CBS-Q//MP2/6-31G(d′) and Max{CBS-Q}//IRC{MP2/6-31G(d′)} energies maximize at the same geometry (Table 5) for the $CH_4 + HO_2$ reaction and thereby give rise to a zero-point-corrected barrier height of 24.27 kcal mol^{-1}. Malick et al. [74] recommended an empirical correction

Table 2. Calculated CBS-Q barrier heights (kcal mol^{-1}) and heats of reaction (kcal mol^{-1})

System	E_0 barrier	ΔH^0_R
$H_2O_2 \rightarrow H + HO_2$		86.71
$H_2 \rightarrow 2H$		104.45
$OH \rightarrow O + H$		101.58
$CH_4 + HO_2 \rightarrow CH_3 + H_2O_2$	24.27	17.02
$CH_3CH_3 + HO_2 \rightarrow CH_3CH_2 + H_2O_2$	18.53	13.24
$CH_3CH_2CH_3 + HO_2 \rightarrow CH_3CH_2CH_2 + H_2O_2$	18.73	13.61
$CH_3(CH_2)_2CH_3 + HO_2 \rightarrow CH_3(CH_2)_2CH_2 + H_2O_2$	18.58	13.60
$CH_3(CH_2)_3CH_3 + HO_2 \rightarrow CH_3(CH_2)_3CH_2 + H_2O_2$	18.19	13.92
$(CH_3)_2CHCH_3 + HO_2 \rightarrow (CH_3)_2CHCH_2 + H_2O_2$	18.40	14.34
$(CH_3)_3CCH_3 + HO_2 \rightarrow (CH_3)_3CCH_2 + H_2O_2$	18.61	14.97
$(CH_3)_3CH + HO_2 \rightarrow (CH_3)_3C + H_2O_2$	11.13	9.22
$(CH_3)_2CHEt + HO_2 \rightarrow (CH_3)_2CEt + H_2O_2$	10.84	9.60
$CH_4 + O \rightarrow CH_3 + OH$	9.42	2.08
$CH_3CH_3 + O \rightarrow CH_3CH_2 + OH$	5.52	−1.70
$CH_3CH_2CH_3 + O \rightarrow CH_3CH_2CH_2 + OH$	5.42	−1.33
$CH_3(CH_2)_2CH_3 + O \rightarrow CH_3(CH_2)_2CH_2 + OH$	5.18	−1.34
$(CH_3)_2CHCH_3 + O \rightarrow (CH_3)_2CHCH_2 + OH$	5.09	−0.60
$(CH_3)_3CCH_3 + O \rightarrow (CH_3)_3CCH_2 + OH$	4.96	0.02
$CH_3OH + H \rightarrow CH_2OH + H_2$	7.40	−9.24
$CH_3OCH_3 + H \rightarrow CH_2OCH_3 + H_2$	6.81	−9.22
$CH_3OEt + H \rightarrow CH_2OEt + H_2$	6.65	−9.22
$CH_3Oi\text{-}Pr + H \rightarrow CH_2Oi\text{-}Pr + H_2$	6.41	−9.80
$CH_3Ot\text{-}Bu + H \rightarrow CH_2Ot\text{-}Bu + H_2$	5.90	−10.27
$CH_3OOH + H \rightarrow CH_2OOH + H_2$	8.25	−7.16
$CH_3OOCH_3 + H \rightarrow CH_2OOCH_3 + H_2$	7.73	−7.70
$CH_3OC(O)H + H \rightarrow CH_2OC(O)H + H_2$	10.19	−5.16
$CH_3OC(O)CH_3 + H \rightarrow CH_2OC(O)CH_3 + H_2$	9.70	−5.57

Table 3. The MP2/6-31G(d′) (the geometry used in CBS-Q) optimized bond lengths (Å) and bond angles (degres) of the reactive moiety in the transition structures and the magnitude of the imaginary frequency. The abstracted hydrogen is indicated in *boldface*

Transition structure	C–H	O–H	C–H–O	$< S^2 >$	ν (cm^{-1})
$\mathbf{CH_4} + HO_2$	1.333	1.161	175.5	0.797	3,396
$CH_3\mathbf{CH_3} + HO_2$	1.311	1.185	173.0	0.798	3,329
$CH_3CH_2\mathbf{CH_3} + HO_2$	1.316	1.181	172.8	0.798	3,381
$CH_3(CH_2)_2\mathbf{CH_3} + HO_2$	1.314	1.182	172.4	0.798	3,338
$CH_3(CH_2)_3\mathbf{CH_3} + HO_2$	1.315	1.183	172.6	0.798	3,337
$(CH_3)_2CH\mathbf{CH_3} + HO_2$	1.314	1.185	171.7	0.798	3,329
$(CH_3)_3C\mathbf{CH_3} + HO_2$	1.312	1.187	176.8	0.798	3,317
$(CH_3)_3\mathbf{CH} + HO_2$	1.273	1.226	172.8	0.799	3,222
$(CH_3)_2\mathbf{CH}Et + HO_2$	1.269	1.232	173.1	0.799	3,224
$\mathbf{CH_4} + O$	1.327	1.165	177.1	2.053	2,960
$CH_3\mathbf{CH_3} + O$	1.303	1.190	176.1	2.054	2,922
$CH_3CH_2\mathbf{CH_3} + O$	1.305	1.189	174.2	2.054	2,918
$CH_3(CH_2)_2\mathbf{CH_3} + O$	1.306	1.188	175.9	2.054	2,921
$(CH_3)_2CH\mathbf{CH_3} + O$	1.306	1.191	175.0	2.054	2,903
$(CH_3)_3C\mathbf{CH_3} + O$	1.306	1.192	175.7	2.053	2,893
$(CH_3)_3\mathbf{CH} + O$	1.296	1.237	178.5	2.053	2,811
$(CH_3)_2\mathbf{CH}Et + O$	1.296	1.237	176.2	2.053	2,830
$\mathbf{CH_3}OH + H$	1.374	0.929	178.1	0.789	2,277
$\mathbf{CH_3}OCH_3 + H$	1.383	0.926	178.1	0.788	2,260
$\mathbf{CH_3}OEt + H$	1.382	0.926	178.1	0.788	2,256
$\mathbf{CH_3}Oi\text{-}Pr + H$	1.378	0.930	177.9	0.788	2,257
$\mathbf{CH_3}Ot\text{-}Bu + H$	1.373	0.931	178.2	0.788	2,266
$\mathbf{CH_3}OC(O)H + H$	1.398	0.898	177.6	0.788	2,337
$\mathbf{CH_3}OC(O)CH_3 + H$	1.396	0.901	177.5	0.788	2,326
$\mathbf{CH_3}OOH + H$	1.389	0.916	177.3	0.788	2,284
$\mathbf{CH_3}OOCH_3 + H$	1.389	0.915	178.7	0.788	2,285

of 0.57 kcal mol^{-1} to the barrier height with the CBS-Q//IRCMAX method and this would place the CBS-Q upper bound at 23.7 kcal mol^{-1}. Simple CBS-QB3 and B3LYP/CBSB3 methods underestimate this barrier height by 2 kcal mol^{-1} (Table 4) which, however, is because of the incorrect geometry. The barrier at the

Table 4. Comparison of the optimized bond lengths (Å) and bond angles (degrees) of the reactive moiety in selected transition structures at various levels and the magnitude of the barrier (kcal mol^{-1}) and the imaginary frequency. The abstracted hydrogen is indicated in *boldface*. An *asterisk* indicates frequencies computed at the B3LYP/6-31G(d′)//B3LYP/6-31G(d′) level

Transition structure	C–H	O–H	C–H–O	$< S^2 >$	E_0	ν (cm^{-1})
$CH_4 + HO_2$(CBS-Q)	1.333	1.161	175.5	0.797	24.27	3,396
$CH_4 + HO_2$(G2)	1.309	1.179	176.4	0.801	25.15	3,384
$CH_4 + HO_2$(CBS-QB3)	1.442	1.111	178.5	0.785	22.83	1,430
$CH_4 + HO_2$(B3LYP/CBSB3)	1.416	1.129	178.9	0.757	22.52	1,604
$CH_4 + HO_2$(CBS-QB3//IRC)	1.367	1.178	178.5	0.757	24.02	1,830
$CH_3CH_3 + HO_2$(CBS-Q)	1.311	1.185	173.0	0.798	18.54	3,329
$CH_3CH_3 + HO_2$(CBS-QB3)	1.393	1.146	175.9	0.757	18.13	1,608
$CH_3CH_3 + HO_2$(B3LYP)	1.376	1.163	178.3	0.757	17.93	1,701
$CH_3CH_3 + HO_2$(CBS-QB3//IRC)	1.329	1.193	175.7	0.757	18.83	1,699
$(CH_3)_2CHCH_3 + HO_2$(CBS-Q)	1.314	1.185	171.7	0.798	18.41	3,329
$(CH_3)_2CHCH_3 + HO_2$(CBS-QB3)	1.394	1.146	174.3	0.757	17.75	1,606
$(CH_3)_2CHCH_3 + HO_2$(B3LYP/CBSB3)	1.380	1.161	178.5	0.757	18.55	1,429*
$(CH_3)_3CH + HO_2$(CBS-Q)	1.273	1.226	172.8	0.799	11.13	3,222
$(CH_3)_3CH + HO_2$(CBS-QB3)	1.337	1.196	176.8	0.757	11.62	1,638
$(CH_3)_3CH + HO_2$(B3LYP/CBSB3)	1.328	1.212	179.6	0.757	12.30	1,611*
$(CH_3)_3CH + HO_2$(CBS-QB3//IRC)	1.278	1.246	179.4	0.757	12.20	1,450
$CH_4 + O$(CBS-Q//IRC)	1.261	1.214	178.3	2.044	9.95	2,267
$CH_4 + O$(CBS-Q)	1.327	1.165	177.1	2.053	9.42	2,960
$CH_4 + O$(G2)	1.306	1.182	177.4	2.054	11.64	2,970
$CH_4 + O$(CBS-QB3)	1.346	1.169	178.5	2.055	9.59	1,434
$CH_4 + O$(B3LYP/CBSB3)	1.318	1.196	179.4	2.010	3.93	1,457
$CH_4 + O$(CBS-QB3//IRC)	1.284	1.219	179.4	2.009	10.05	1,332

Max{CBS-QB3}//IRC {B3LYP/CBSB7} level is in good agreement with the Max{CBS-Q}//IRC{MP2/6-31G(d′)} barrier: by moving along the B3LYP reaction coordinate to the real maximum in the CBS-QB3 energy we get a much better estimate. We observe an improved agreement between the CBS-Q//MP2/6-31G(d′) and Max{CBS-QB3}// IRC{B3LYP/CBSB7} results (Table 4) for primary and tertiary hydrogen abstractions as well.

The drastic difference between the B3LYP and the molecular-orbital-based methods can also be seen in the wildly different imaginary frequencies predicted using different methods (Table 4). At the HF and MP2 levels, the reaction coordinate corresponds to an asymmetric C–H–O stretch, while at the B3LYP level this mode is strongly coupled with the out-of-plane vibration of the forming radical center. The B3LYP imaginary frequency remains very low even at the IRCMAX geometry, i.e., the B3LYP second derivatives are consistently different from those predicted by other methods over a range of geometries.

There is one somewhat surprising conclusion from these calculations (Table 6): the reverse reaction

$$\text{tertiary} - R + \text{HOOH} \rightarrow R\text{H} + \text{HO}_2$$

is calculated to have a slightly lower barrier than the corresponding reaction of primary alkyl radicals, opposite to the trend in the reaction exothermicity. This would not be unprecedented, as tertiary alkyl radicals have been directly measured in the liquid phase to have higher reactivity than other alkyl radicals in the exothermic hydrogen abstractions from silanes [202] and stannanes [203]. However, in many systems it is clear that tertiary radical is less reactive than the primary. We fear this calculated barrier might be sensitive to errors in the theoretical estimation of the ΔH_f of the *t*-butyl radical. The heat of formation of the *t*-butyl radical has been the subject of considerable debate between proponents of "low" (approximately 9 kcal mol^{-1}) and "high" (approximately 12 kcal mol^{-1}) values. A value of 12.30 kcal mol^{-1} was recommended by Berkowitz et al. [204], while the value recommended by Tsang in the NIST webbook is 11 kcal mol^{-1}. On the basis of high-level theoretical calculations, Smith and Radom [205] recommended a value of 13.6 ± 1.7 kcal mol^{-1}. The calculated heats of formation in the present work at the CBS-Q and CBS-QB3 levels are, respectively, 13.20 and 12.41 kcal mol^{-1}. However, if the low value for ΔH_f were correct, then the barrier to tertiary radical abstraction would be higher and the reaction would be slower (in accord with the trend in reaction exothermicity). We are unable to resolve this longstanding dispute.

All our high-level calculations for the $HO_2 + RH$ TS appear to converge near the values obtained by the CBS-Q method, which (while not cheap) is relatively inexpensive compared to comparably accurate alternatives.

3.3.2 Detailed discussion of the TS for abstractions by $O(^3P)$

The reaction $CH_4 + O(^3P) \rightarrow CH_3 + OH$ is theoretically challenging [206, 207, 208] as the approach of $O(^3P)$ along a C–H bond has threefold symmetry and leads to a Jahn–Teller conical intersection rather than a saddle point. The computed barrier height for this reaction varies from 37.5 to −2.8 kcal mol^{-1}, while experimental results suggest a barrier of 9−11.4 kcal mol^{-1}. The barrier heights calculated at the CBS-Q (9.4 kcal mol^{-1}) and G2 (11.6 kcal mol^{-1}) levels are, respectively, at the lower and upper ends of the experimental range. Jursic [207] demonstrated in his work the drastic failure of all DFT methods to accurately predict this barrier. We

Table 5. The geometry of the reactive moiety along the intrinsic reaction coordinate (*IRC*) path for different selected reactions along with the low-level *E*(IRC) [*E*(B3LYP/CBSB7) or *E*(MP2/6-31G(d′)] and high-level energies [*E*(CBS-QB3) or *E*(CBS-Q)] (au)

R_{C-H}	R_{O-H}	*E*(low-level)	*E*(high-level)
$CH_4 + HO_2$(CBS-QB3//IRC{B3LYP/CBSB7})			
1.482	1.081	–191.44422	–191.116083
1.441	1.110	–191.44402	–191.114689
1.401	1.139	–191.44427	–191.113474
1.369	1.181	–191.44511	–191.112786
1.327	1.209	–191.44661	–191.113110
1.295	1.249	–191.44874	–191.114213
$CH_4 + HO_2$(CBS-Q//IRC{MP2/6-31G(d′)})			
1.215	1.257	–190.79169	–191.113225
1.270	1.208	–190.7878	–191.110009
1.333	1.160	–190.78643	–191.109041
1.397	1.113	–190.78763	–191.110229
1.467	1.069	–190.79054	–191.112158
1.537	1.031	–190.79391	–191.113407
$C_2H_6 + HO_2$(CBS-QB3//IRC{B3LYP/CBSB7})			
1.216	1.292	–230.77946	–230.343773
1.269	1.242	–230.77666	–230.342094
1.328	1.193	–230.77469	–230.341605
1.393	1.145	–230.77401	–230.342709
1.459	1.098	–230.77458	–230.344952
1.528	1.057	–230.77595	–230.346864
$(CH_3)_3CH + HO_2$(CBS-QB3//IRC{B3LYP/CBSB7})			
1.226	1.295	–309.43512	–308.806220
1.278	1.246	–309.43369	–308.806137
1.336	1.197	–309.43313	–308.807046
1.399	1.148	–309.43374	–308.808960
1.465	1.101	–309.43534	–308.811382
CH_4 + O(CBS-QB3//IRC{B3LYP/CBSB7})			
1.184	1.319	–115.60748	–115.382531
1.227	1.269	–115.60611	–115.382003
1.283	1.218	–115.60497	–115.381615
1.346	1.169	–115.60452	–115.382362
1.412	1.122	–115.60498	–115.384143
1.482	1.078	–115.60613	–115.385934
CH_4 + O(CBS-Q//IRC{MP2/6-31G(d′)})			
1.538	1.033	–115.18571	–115.385253
1.465	1.071	–115.18267	–115.384279
1.393	1.116	–115.18004	–115.382612
1.327	1.165	–115.17895	–115.381632
1.261	1.214	–115.18014	–115.380783
1.203	1.265	–115.18330	–115.381161

observe a similar failure in classical barrier height (3.93 kcal mol^{-1}) predictions at the B3LYP/CBSB3 level; however, the compound CBS-QB3 procedure based on the B3LYP geometry overcomes this failure and the computed Max{CBS-QB3}//IRC{B3LYP/CBSB7} and Max{CBS-Q}//IRC{MP2/6–31G(d′)} upper bounds for the classical barrier heights are, respectively, 10.0 and 9.95 kcal mol^{-1} (Table 4). Incorporation of Petersson's empirical correction to the latter reduces it to 9.4 kcal mol^{-1}. This reaction, consequently, provides a sample case to demonstrate the weakness of the TS GA method: the supergroup values are only as good as the quantum chemical TSs on which they are based. Sometimes considerable effort must be made by the researchers to find the appropriate level of theory for the proper description of transition structures. This task becomes a difficult and intuitive one when experimental rate data are scarce and the quantum chemistry predictions change dramatically depending on the method used.

3.4 Supergroup thermochemical values and their transferability

Reaction family rate prediction is meaningful only if the parameters for the reactive moiety are transferable among the members of a given reaction family. To test whether the supergroup thermochemical values are transferable, we derived them from quantum chemical CBS-Q calculations on more than one reaction in each family.

In Tables 7 and 8, we present the thermochemical values of the reactive moiety for the individual reactions as well as the average for a specific reaction type, viz., supergroup parameters at the CBS-Q level. A quick glance reveals that the contributions from the reactive moiety remains essentially the same for all the members in the {C/C/H2/-H/O/O} and {C/C/H2/-H/O(^{3}P)} reaction families. We compare the reaction rates based on supergroups with the individual TST rates for the $RH + HO_2$ reaction in Fig. 1. In this figure, we present

Table 6. Comparison of calculated heat of reaction, forward, and reverse barrier heights at different levels of theory for methyl, primary, and tertiary hydrogen abstractions by HO_2. All in kcal/mol

Reaction	Method	Forward E_0	Reverse E_0	ΔH_R
$CH_4 + HO_2 \rightarrow CH_3 + H_2O_2$	CBS-Q	24.28	7.25	17.02
	CBS-QB3	22.83	5.58	17.25
	Max{CBS-QB3}	24.02	6.77	
	Max{CBS-Q}	24.28	7.25	
	B3LYP/CBSB3	22.52	2.67	19.85
$C_2H_6 + HO_2 \rightarrow C_2H_5 + H_2O_2$	CBS-Q	18.54	5.30	13.24
	CBS-QB3	18.13	4.78	13.36
	Max{CBS-QB3}	18.84	5.48	
	B3LYP/CBSB3	17.93	2.87	15.06
$i\text{-}C_4H_{10} + HO_2 \rightarrow t\text{-}C_4H_9 + H_2O_2$	CBS-Q	11.13	1.91	9.22
	CBS-QB3	11.62	2.90	8.72
	Max{CBS-QB3}	12.19	3.47	
	B3LYP/CBSB3	12.30	3.71	8.59

Table 7. Group additivity values for transition-state "supergroups" for $HO_2 + RH$ in kcal/mol and cal/mol K units. The name of the supergroup and the abstracted hydrogen in each reaction are given in *boldface*. Unless noted otherwise, the values are derived from CBS-Q calculations

Reactions/supergroups	ΔH_f	$S^{(298)}$	C_p^{300}	C_p^{400}	C_p^{500}	C_p^{600}	C_p^{800}	$C_p^{1,000}$	$C_p^{1,500}$
{C/H3/—H/O/O}									
$\mathbf{CH_4} + HO_2$(CBS-Q(HO))	25.19	47.47	12.31	14.75	16.81	18.55	21.39	23.60	26.87
$\mathbf{CH_4} + HO_2$(G2(HO))	26.10	47.71	12.47	14.85	16.87	18.58	21.38	23.57	26.84
$\mathbf{CH_4} + HO_2$(CBS-QB3(HO))	23.76	47.50	12.53	15.00	17.03	18.73	21.52	23.69	26.91
$CH_3\mathbf{H_3} + HO_2$	27.72	27.75	10.39	12.94	14.93	16.55	19.10	20.99	23.70
$CH_3CH_2\mathbf{CH_3} + HO_2$	28.21	27.01	10.84	13.26	15.14	16.70	19.17	21.02	23.69
$CH_3(CH_2)_2\mathbf{CH_3} + HO_2$	28.15	27.57	10.67	13.12	15.04	16.60	19.08	20.93	23.63
$CH_3(CH_2)_3\mathbf{CH_3} + HO_2$	28.03	27.21	11.15	13.49	15.28	16.75	19.13	20.95	23.63
$(CH_3)_2CH\mathbf{CH_3} + HO_2$	27.80	27.56	10.27	12.81	14.81	16.42	18.95	20.82	23.54
$(CH_3)_3C\mathbf{CH_3} + HO_2$	28.13	27.22	11.08	13.60	15.50	17.00	19.35	21.12	23.71
{C/C/H2/—H/O/O}	28.01	27.39	10.73	13.20	15.11	16.67	19.13	20.97	23.65
Range	0.49	0.75	0.89	0.79	0.69	0.58	0.40	0.30	0.17
$(CH_3)_3C\mathbf{H} + HO_2$	28.31	−14.52	9.79	11.43	12.59	13.51	14.92	15.82	17.04
$(CH_3)_2CEt\mathbf{H} + HO_2$	28.34	−14.67	9.66	11.52	12.79	13.74	15.09	15.92	17.05
{C/C3/—H/O/O}	28.33	−14.59	9.72	11.48	12.69	13.62	15.00	15.87	17.05
Range	0.03	0.15	0.14	0.09	0.21	0.23	0.17	0.10	0.01

the relative difference of rates for tunneling-corrected individual reaction rates, k^{TST}, compared to the GA-based rate prediction, k^{GA}. The GA rates are calculated via

$$\Delta G^{\neq} = G\{\mathrm{C/C/H2/-\,H/O/O}\} + G\{\mathrm{O/O/H}\} - G\{\mathrm{C/C/H3}\} - G\{\mathrm{HO2}\}, \quad (23)$$

$$k^{GA} = \left[1 + \frac{1}{24}\left(\frac{1.44 v_{ave}}{T}\right)^2\right] \frac{V_m k_B T}{h} \exp\left(-\Delta G^{\neq}/RT\right), \quad (24)$$

where v_{ave} is the average magnitude of the imaginary frequency over the calculated TSs in a single reaction family. In the present case, the molar volume $V_m = RT/P_0$, where $P_0 = 1$ atm. The TST rates are obtained from Eq. (4). The rates in Fig. 1 are per abstractable hydrogen. A deviation of +100% means that the TST rate is a factor of 2 larger than the GA rate, while a deviation of −50% implies a factor of 2 smaller than the GA rate. Figure 1 shows that all TST rates are within a factor of 2 of the GA predictions. Despite some deviations, the overall constancy and consistency of the supergroup is good, and with increasing temperatures the rate approaches the GA rate. In other words, with nonpolar alkyl substituents, the interaction of the unreactive moiety with the reactive moiety remains the same in the reactant as well as in the transition structure even in an endothermic reaction set.

The supergroup value is not constant in the reaction series $CH_3OX + H \rightarrow CH_2OX + H_2$ (Table 8). The substituent X alters the β C–H bond strength as well as the barrier height. It is coupled to the reactive moiety through the mediating oxygen atom. When X is varied from *n*-alkyl (Me, Et) to *i*-Pr to *t*-Bu, the barrier height as well as the BDE decreases (Table 2). Increased branching increases the steric crowding at the reaction center. If one calculates the inductive effect of the substituents using Cherkasov's atomic additivity rules, all O*R* substituents have nearly the same inductive influence (1.72), which is slightly more than the OH group (1.70). The fact that the computed barrier height decreases while going from OMe to O*t*-Bu suggests steric contributions to the barrier height are important. The significant jump in the barrier height from O*R* to either OC(O)*R* (inductive parameter 2.3) or OO*R* reflects the inductive involvement to the barrier height. The calculated inductive and steric parameters of the substituents are tabulated in Table 9. One can arrive at multilinear expressions for the barrier height based on

Table 8. Group additivity values for transition-state supergroups for hydrogen abstraction from alkanes by O(^{3}P), from CH_3OX by H, and from symmetric reactions such as $H + H_2$, $CH_3 + CH_4$, $C_2H_5 + C_2H_6$, *i*-C_4H_{10} + *t*-C_4H_9, and $HO_2 + H_2O_2$ The name of the supergroup and the abstracted hydrogen in each reaction are given in *boldface*. Unless noted otherwise, all values are derived from CBS-Q calculations

Reactions/supergroups	ΔH_f	$S^{(298)}$	C_p^{300}	C_p^{400}	C_p^{500}	C_p^{600}	C_p^{800}	$C_p^{1,000}$	$C_p^{1,500}$
{C/H3/—H/O}									
CH_4 + O(CBS-Q)	50.28	63.18	13.70	15.78	17.58	19.06	21.36	23.09	25.81
CH_4 + O(G2)	52.56	63.62	13.86	15.89	17.64	19.08	21.34	23.06	25.78
CH_4 + O(CBS-QB3)	50.37	62.69	13.40	15.53	17.36	18.88	21.25	23.03	25.80
CH_3CH_3 + O	54.48	43.58	11.28	13.56	15.36	16.79	18.89	20.34	22.57
CH_3CH_3 + O(G2)	57.18	43.54	11.23	13.52	15.32	16.76	18.87	20.34	22.57
$CH_3CH_2CH_3$ + O	54.53	42.73	11.68	13.90	15.61	16.96	18.97	20.38	22.57
$CH_3(CH_2)_2CH_3$ + O(G2)	57.33	42.70	11.65	13.86	15.58	16.94	18.96	20.38	22.57
$CH_3(CH_2)_2CH_3$ + O	54.34	43.34	11.35	13.62	15.41	16.82	18.89	20.33	22.54
$(CH_3)_2CHCH_3$ + O	54.29	42.76	11.49	13.74	15.48	16.84	18.87	20.31	22.53
$(CH_3)_3CCH_3$ + O	54.05	42.89	11.42	13.79	15.61	17.02	19.07	20.47	22.63
{C/C/H2/—H/O}	54.34	43.06	11.44	13.72	15.49	16.89	18.94	20.37	22.57
Range	0.48	0.85	0.41	0.33	0.25	0.24	0.29	0.17	0.10
CH_3OH + H	48.30	36.79	9.85	12.57	14.70	16.35	18.62	20.19	22.48
CH_3OOH + H	49.44	36.72	10.14	12.71	14.84	16.51	18.80	20.35	22.58
CH_3OOCH_3 + H	48.90	37.90	9.87	12.50	14.64	16.32	18.64	20.24	22.55
CH_3OCH_3 + H	47.81	38.16	9.60	12.34	14.57	16.27	18.59	20.15	22.44
$CH_3OCH_2CH_3$ + H	47.69	37.32	9.52	12.21	14.48	16.24	18.59	20.15	22.44
$CH_3OCH(CH_3)_2$ + H	47.86	37.88	9.84	12.71	14.90	16.54	18.73	20.23	22.46
$CH_3OC(CH_3)_3$ + H	47.77	37.43	9.90	12.40	14.44	16.07	18.38	19.99	22.37
$CH_3OC(O)H$ + H	51.30	37.45	10.30	12.83	14.93	16.58	18.81	20.26	22.36
$CH_3OC(O)CH_3$ + H	50.77	37.12	10.10	12.61	14.68	16.36	18.74	20.34	22.47
{C/O/H2/—H/H}		37.57	9.90	12.54	14.69	16.36	18.66	20.21	22.46
Range		1.44	0.78	0.62	0.48	0.51	0.43	0.35	0.22
$H + H_2$(**2{H/—H}**)	60.35	39.13	7.62	8.49	9.26	9.91	10.88	11.51	12.31
$CH_3 + CH_4$(**2{C/H3/—H}**)	32.54	68.74	16.36	19.64	22.68	25.36	29.76	33.17	38.67
$C_2H_5 + C_2H_6$(**2{C/C/H2/—H}**)	43.60	28.62	12.29	15.79	18.73	21.21	25.14	27.99	32.36
i-C_4H_{10} + *t*-C_4H_9 (**2{C/C3/—H}**)	48.55	−56.92	12.53	14.19	15.32	16.23	17.49	18.12	19.23
$H_2O_2 + HO_2$(**2{O^p/—H/O^p}**)	13.48	21.14	10.35	11.90	12.65	13.12	13.75	14.17	14.71

inductive and steric parameters of O*X*, viz., $E_0(X) = E_0(H) + a_1\sigma + a_2R_s$, as presented in our earlier work [188] and arrive at rate rules with modified ΔH of the supergroup, where $E_0(H)$ is the barrier height for the hydrogen substitutent. Such multilinear expressions will be presented elsewhere. Alternatively, the barrier height seems to correlate well with the bond strength except for $X = OH$ (Fig. 2). One can use a linear Evans–Polanyi relationship to obtain the zero-point-corrected barrier height, $E_0(X) = 14.206 + 0.8113\Delta H_{rxn}$ and in turn the substituent-dependent enthalpy of the supergroup.

The substituent dependence of ΔH_{rxn} can easily be computed using conventional GA methods for thermochemistry [2].

3.5 Comparison of supergroup predicted rate with literature data

3.5.1 HO_2 + *R*H reactions

Walker [209] studied HO_2 radical reactions and explained the absolute reactivity of various C–H sites. The rate expressions given by Walker are based primarily on data near 750 K [210] and estimates regarding temperature dependence. Tsang and Hampson [211, 212] arrived at the temperature dependence of 1°, 2°, and 3° rate constants using BEBO calculations. Their recommended expression for the rate constants is supported by Baldwin et al. [210] from their studies on tetramethylbutane and HO_2. Baulch et al. [213] gave recommended values based on these data. It is not trivial to extract the absolute rate constants and their temperature dependence from the available data, much of it taken in rather complex multicomponent reacting systems.

We compare the predicted rates for the $CH_4 + HO_2$ reaction with kinetic data from the NIST database [214] and with rate constants used in the models of Curran et al. [215], the Leeds model of Hughes et al. [216], Konnov [217], Hidaka et al. [218], Miller and Bowman [219], and Ranzi et al. [220] in Fig. 3. Rate comparison is restricted to temperatures between 300 and 1,500 K, the range for which GA C_p values are available. Our GA predicted rate is in very good agreement with recommendations of Baulch et al. [213] at low temperature and at high temperatures it is slightly higher than the references. The differences are largest with respect to the rates of Tsang, followed by those of Ranzi et al. Miller and Bowman used the recommendation of Tsang, while the mechanisms of Konnov, Hidaka, and the Leeds model use the recommendation of Baulch et al. For the reaction of primary C–H with the HO_2 radical, as can be seen from Fig. 4, our prediction lies between the literature estimates at low temperatures and is in good agreement with the recommendations of Tsang and Baulch et al. at high temperatures. The rate for tertiary hydrogen abstraction by the HO_2 radical is not well con-

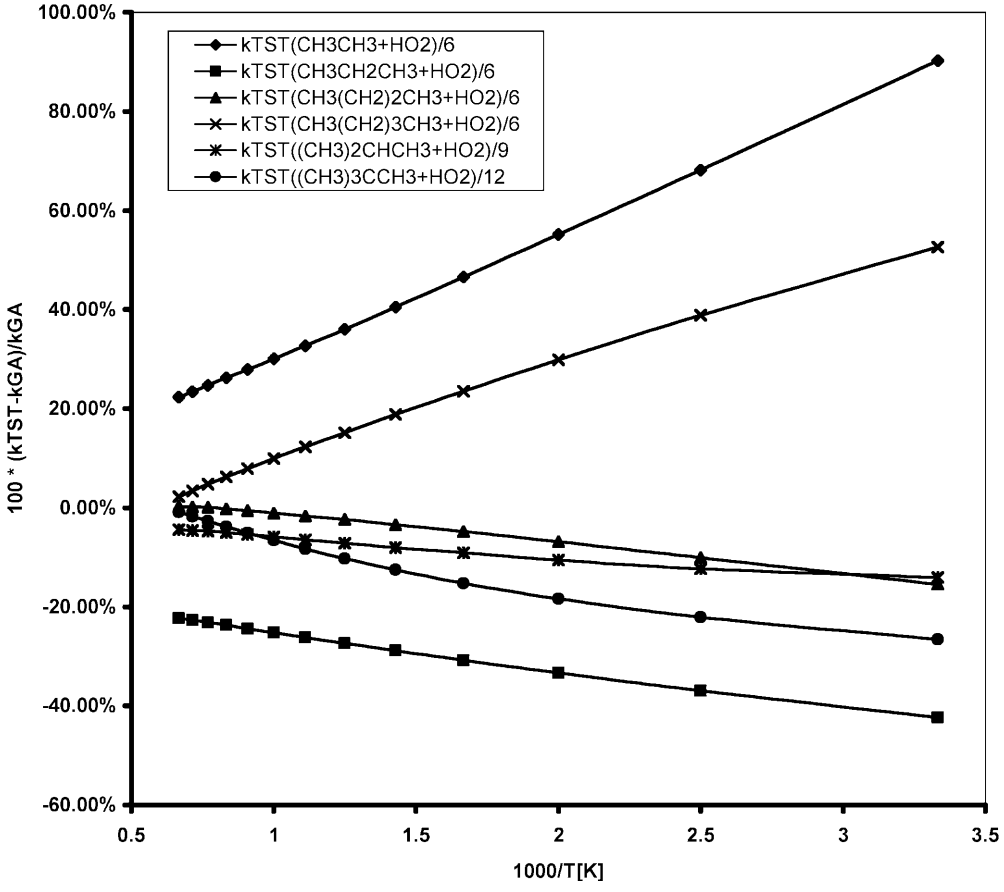

Fig. 1. Comparison of individual transition-state-theory (*TST*) rates with the rate predicted using group additivity for hydrogen abstraction by HO_2 from primary C–H bonds

Table 9. Calculated inductive (σ^*) and steric (R_s) parameters of substituents

Substituent	σ^*	R_s
OH	1.699	−1.07
OCH_3	1.719	−1.537
OCH_2CH_3	1.719	−1.745
$OCH(CH_3)_2$	1.719	−2.041
$OC(CH_3)_3$	1.719	−2.38
OC(O)H	2.830	−1.618
$OC(O)CH_3$	2.862	−1.835
OOH	2.332	−1.373
$OOCH_3$	2.334	−1.639

strained by experimental data, and literature estimates vary widely (Fig. 5). Tsang's prediction has a quoted uncertainty factor of 10 at higher temperatures and our estimate lies within that error bar. It is obvious from Fig. 5 that the temperature dependence is quite different among these different estimates; this reflects different assumed values for the tertiary C–H BDE, which has been a matter of continuing controversy in the literature [205]. Our predictions parallel those of Tsang but differ significantly from those of Walker and Lloyd [214], who obtained a lower activation energy and a lower *A* factor.

In the absence of enough experimental data, it is hard to estimate the accuracy of our predictions for HO_2 attack on tertiary C–H bonds; however, in the better-understood cases discussed previously, our predictions are always within a factor of 10 of the best experimental estimates, so it might be reasonable to infer a similar error bar for this case as well.

3.5.2 $O(^3P) + RH$ reactions

Reactions of atomic oxygen (^3P) with alkanes have been extensively studied from 300 to 2,200 K owing to their importance as initial steps in the combustion of hydrocarbons. The recent measurements agree very well over the temperature range from 400 to 2,500 K. The most recent measurements on the rate constants of C_1–C_6 alkanes with atomic oxygen were made by Miyoshi et al. [221] at high temperatures (850−1,250 K) using the laser photolysis–shock tube–atomic resonance absorption method. Cohen and Westberg [222, 223] extensively reviewed experimental data for O plus alkanes and presented recommended rate constants up to 2,000 K. They used TST calculations to extrapolate rate constants to high temperatures and examined the validity of GA of the rate constants, i.e., whether the rate constants for hydrogen-abstraction reactions can be expressed as the sum of site-specific rate constants for primary, secondary, and tertiary sites or not. Corchado et al. [208] reported the variational TST results in curvilinear coordinates with transmission coefficients calculated by the microcanonical optimized multidimensional tunneling approximation. As discussed in the previous section, the barrier heights computed for $CH_4 + O(^3P)$ vary appreciably with the level of theoretical treatment. The barrier height at the CBS-Q and G2 levels differs by 2 kcal mol^{-1} and this would

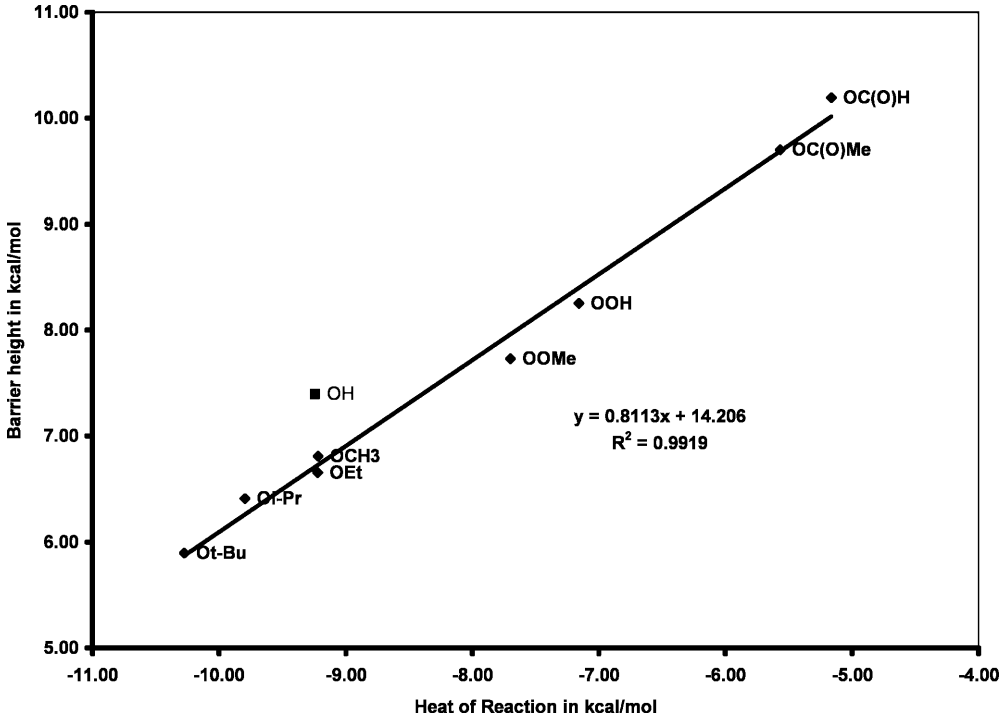

Fig. 2. Evans–Polanyi plot for the $X\mathrm{OCH_3} + \mathrm{H} \rightarrow X\mathrm{OCH_2} + \mathrm{H_2}$ (X = H, Me, Et, *i*-Pr, *t*-Bu, OH, OMe, CHO, $\mathrm{COCH_3}$) reaction

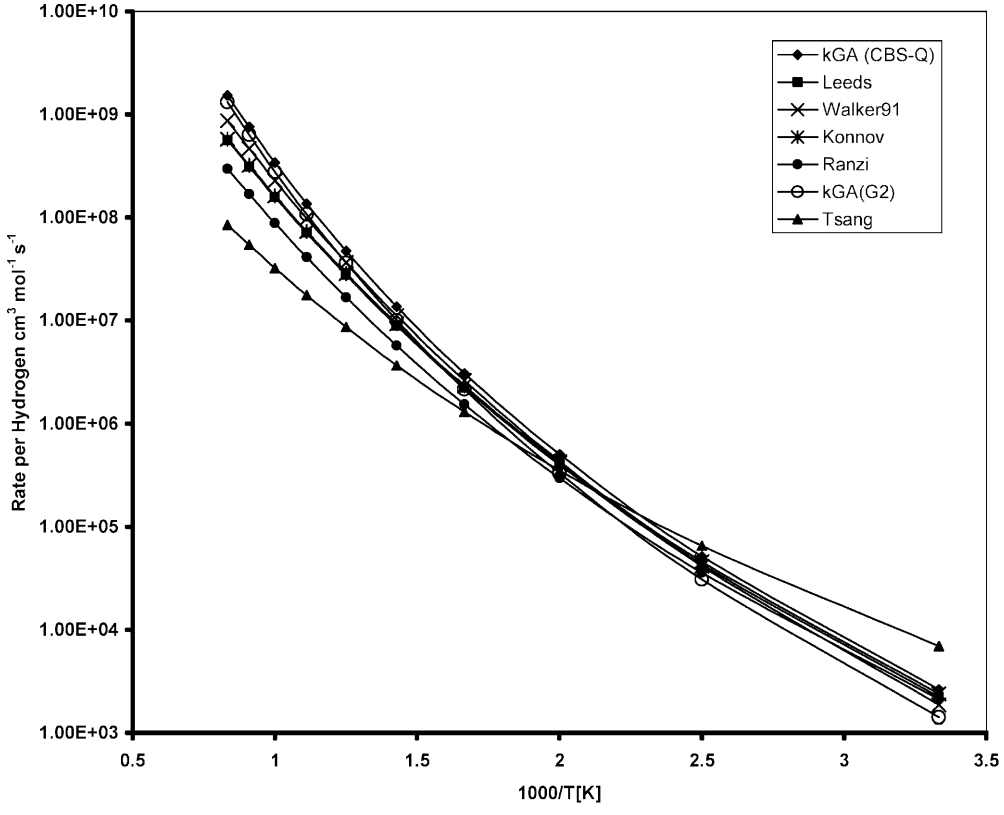

Fig. 3. Comparison of group additivity predicted rates with literature estimates for the $\mathrm{CH_4} + \mathrm{HO_2} \rightarrow \mathrm{CH_3} + \mathrm{H_2O_2}$ reaction

introduce obvious differences in rate predictions at low temperatures. However, the converged upper bound at both CBS-Q//IRC and CBS-QB3//IRC corresponds to 10 kcal $\mathrm{mol^{-1}}$. Consequently, in Fig. 6, we compare our GA estimate corresponding to the upper-bound barrier with TST calculations by Cohen and Westberg [222] and earlier measurements [214]. Before discussing the results of our predictions, it is appropriate to mention the electronic degeneracy of the oxygen atom. The electronic partition function of the oxygen atom $\mathrm{O}(^3\mathrm{P})$,

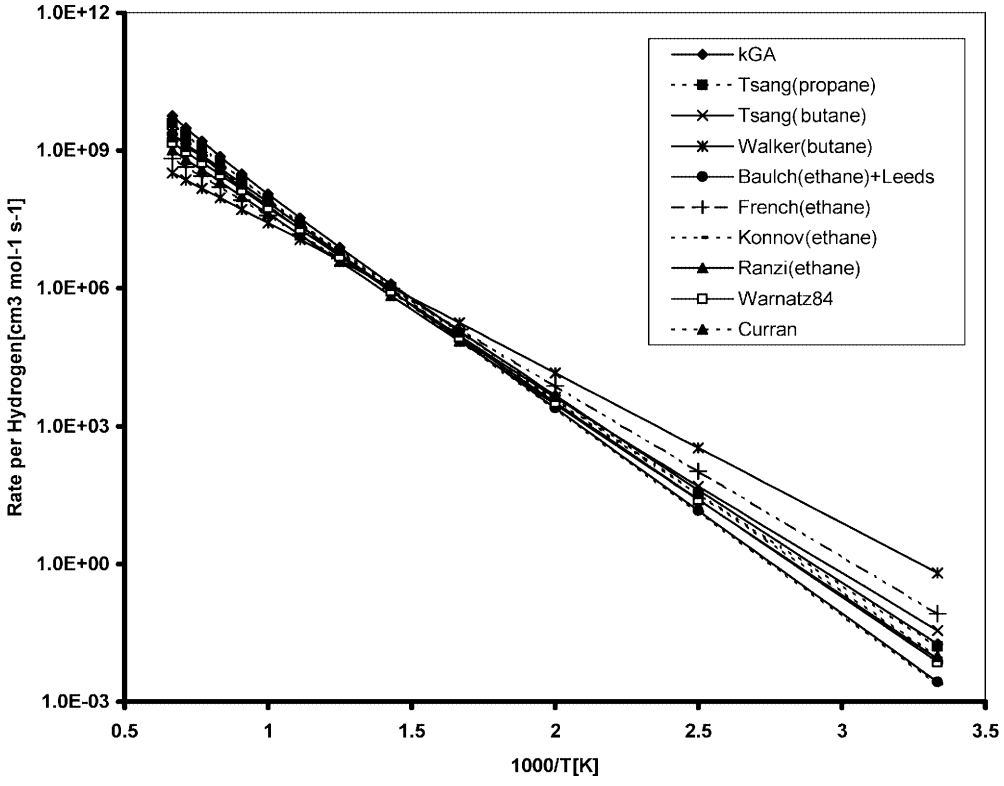

Fig. 4. Comparison of group additivity predicted rates with literature estimates for primary hydrogen abstraction by the HO_2 radical

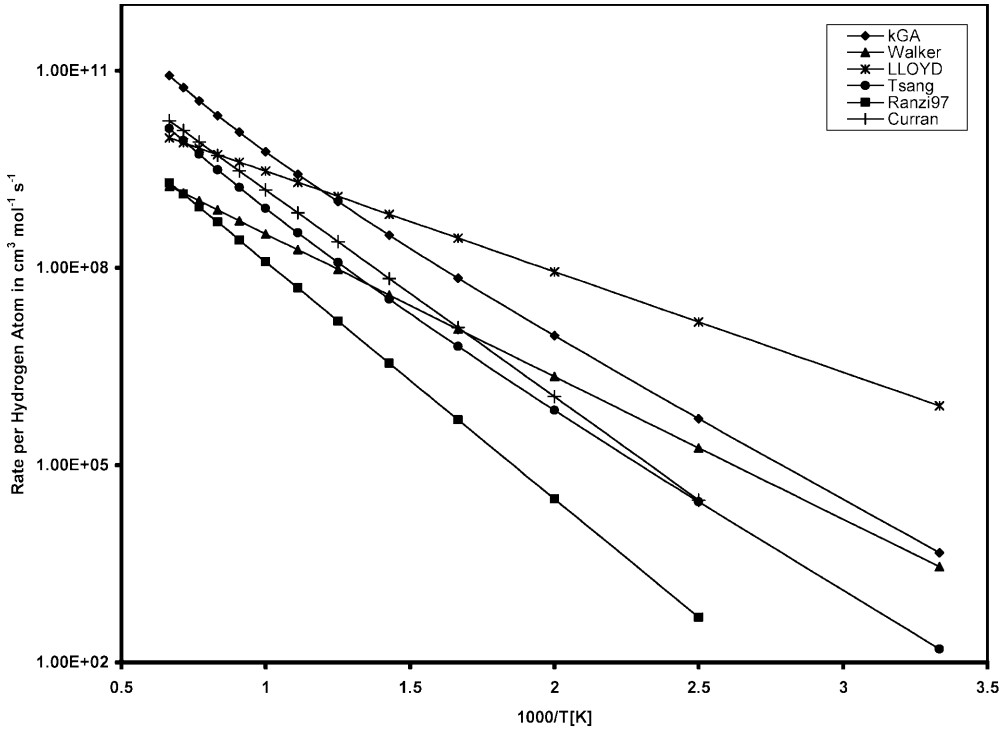

Fig. 5. Comparison of group additivity predicted rates with literature estimates for tertiary C–H abstraction by the HO_2 radical

$$Q_{\text{elec}} = \sum g_i \exp(-\varepsilon_i/RT) = 5 + 3\exp(-228)/T + \exp(-326/T) = 6.98, \tag{25}$$

at 298 K using the known term values and $(2J+1)$ degeneracy factors for the $^3P_2$, $^3P_1$, and $^3P_0$ states. Since in Benson's GA table, a value of 7 was used for the electronic degeneracy at 298 K, we also employed in our computation a constant factor of 7 for the electronic partition function as one would combine this with our supergroups to arrive at the $\Delta G^{\neq}$ of the reaction. Our predictions are in excellent agreement with earlier measurements [214] and TST calculations. The rate

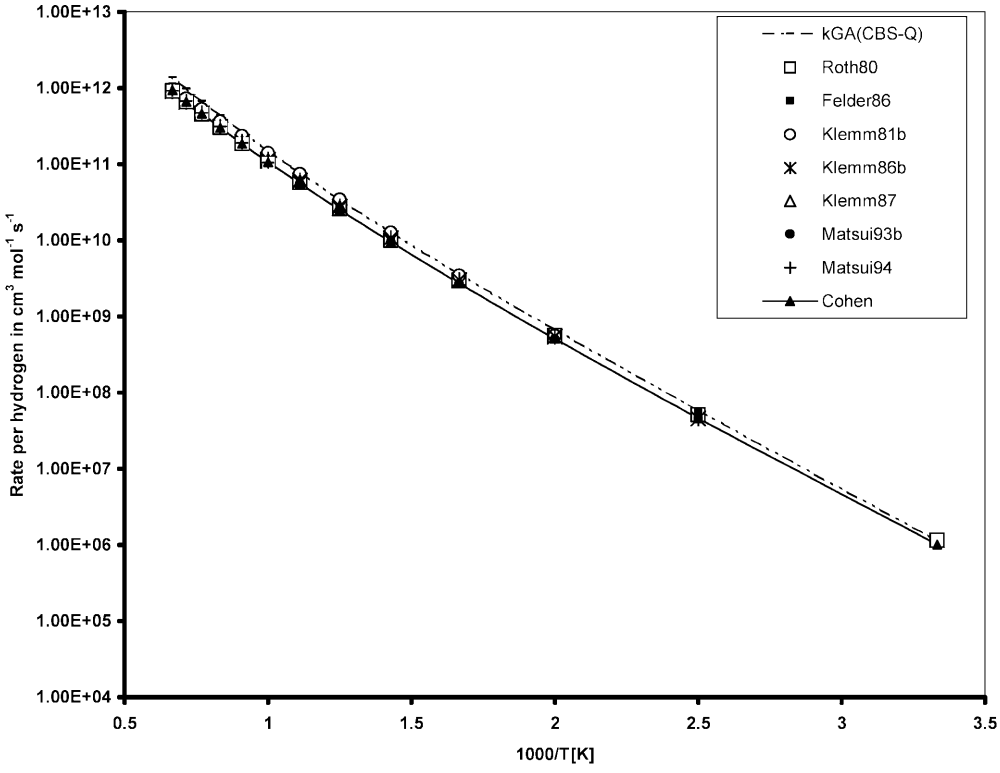

Fig. 6. Comparison of the group additivity predicted rate for the $CH_4 + O(^3P) \rightarrow CH_3 + OH$ reaction with experimental data from the literature

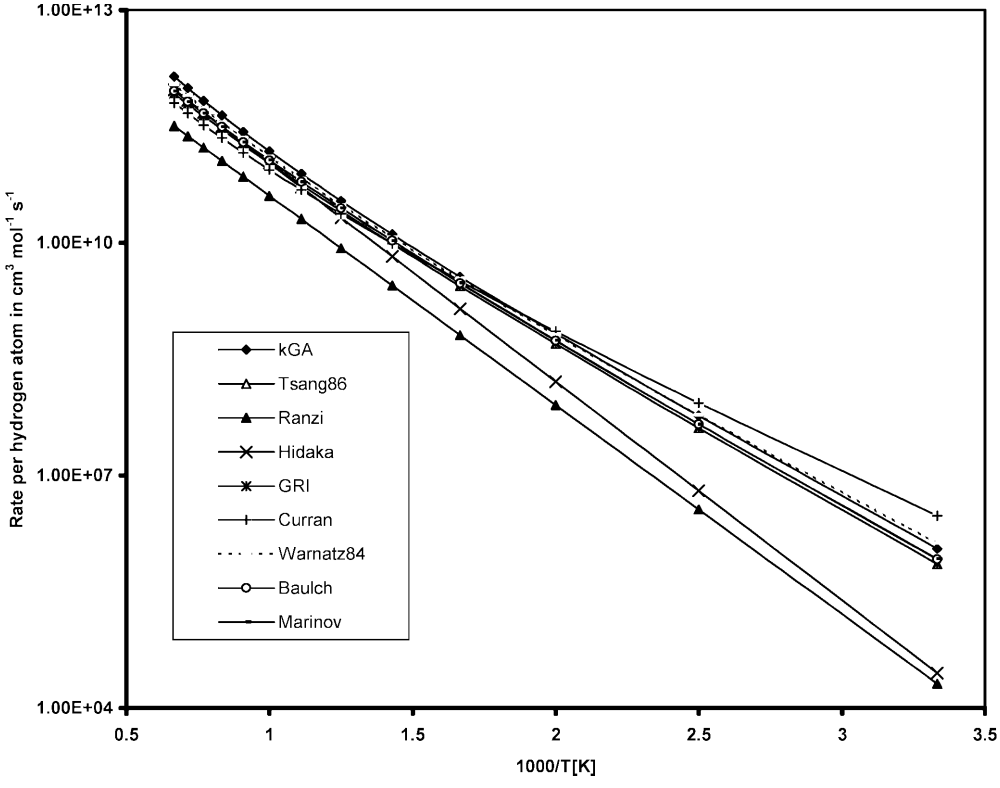

Fig. 7. Comparison of the group additivity predicted rate for the $CH_4 + O(^3P) \rightarrow CH_3 + OH$ reaction with estimates used in accepted kinetic models

estimates used in different mechanisms are compared in Fig. 7 together with our predictions for the $CH_4 + O \rightarrow CH_3 + OH$ reaction. Tsang's predictions are employed in the Gas Research Institute [224] and Miller and Bowman mechanisms, while the recommendations of Baulch et al. are followed in the mechanisms of, Konnov, Marinov and Malte [225], and the Leeds model. Surprisingly the rate estimate employed in Curran's *n*-heptane mechanism follows a different temperature dependence and is nearly a factor of 5 higher than the recommendations of Tsang and Baulch et al. at low temperature. Except for Ranzi's mechanism, all the

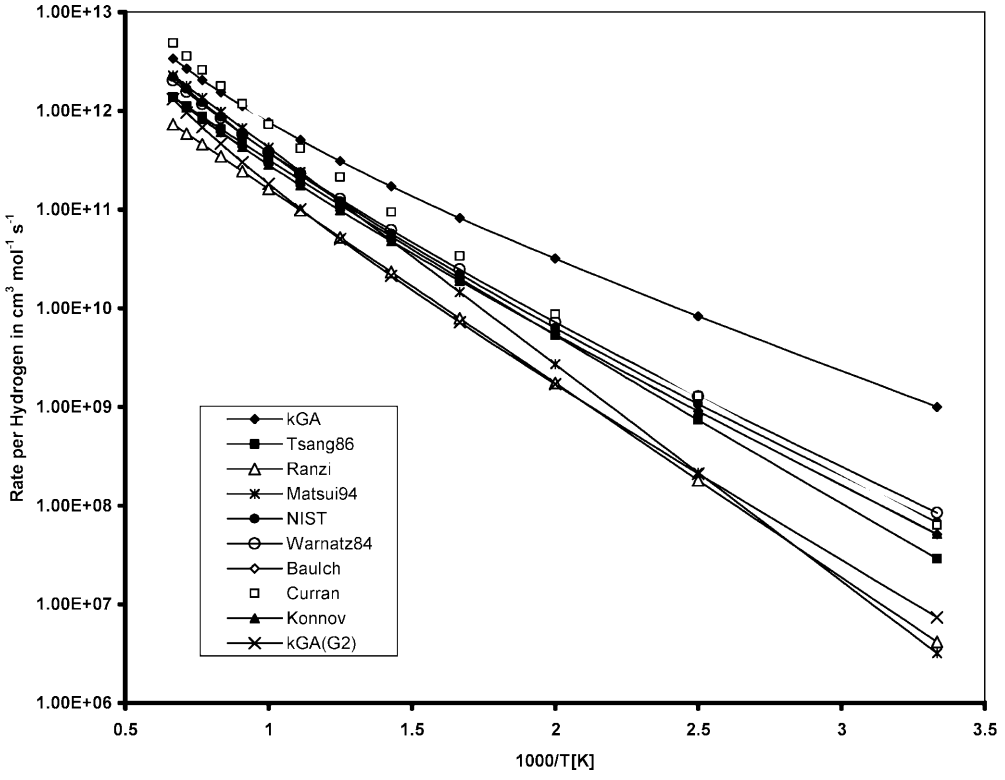

Fig. 8. Comparison of group additivity predicted rate estimate for primary hydrogen abstraction by atomic oxygen (^{3}P) with rate estimates from kinetic models

other mechanisms use a rate estimate which agrees well within a factor of 2 with our predictions.

As shown in Table 2, the computed primary hydrogen abstraction barrier by oxygen from alkanes varies between 5 and 5.5 kcal mol^{-1} at the CBS-Q level, while it is in the range from 8.2 to 8.4 kcal mol^{-1} at the G2 level. The CBS-QB3 barrier height for $C_2H_6 + O$ is 5.94 kcal mol^{-1}. The wide spread in the computed barrier height introduces a big gap in predictions. Comparison with literature estimates [214] (Fig. 8) reveals the predictions at the CBS-Q and G2 levels to be, respectively, the upper and lower bounds for the reaction rate; however, additional IRCMAX calculations or experimental rate constant measurements are needed to establish the barrier height for this class of reaction. To the extent that these reactions are similar to $O + CH_4$, for which we did the IRCMAX calculations, we predict that the true barrier is slightly higher than the CBS-Q value, i.e., about 6 kcal mol^{-1}.

In summary, the rate predictions presented here are reasonable, but tend to be on the high end of available estimates. In the absence of experimental data, it is now possible to arrive at a meaningful a priori rate estimate for any reaction. Since the generic rules are based on the thermochemical properties of the reactive moiety, they are thermodynamically consistent and provide the proper temperature dependence of the rate predictions.

4 Conclusions

An efficient rate-estimation method has been devised combining classical GA and LFER concepts with the wealth of information available from high-level quantum chemical TS calculations. Related previous work has been selectively reviewed. The new method is suitable for high-throughput applications such as computerized kinetic-model construction. Example calculations are presented on the following systems

$$CH_4 + HO_2 \rightarrow CH_3 + H_2O_2 \Rightarrow \{C/H3/-\,H/O/O\},$$

$$RCH_3 + HO_2 \rightarrow RCH_2 + H_2O_2 \quad (R = CH_3, Et, Pr, i\text{-}Pr, t\text{-}Bu) \Rightarrow \{C/C/H2/-\,H/O/O\},$$

$$R_2CR'H + HO_2 \rightarrow R_2CR' + H_2O_2 \quad (R = CH_3, R' = CH_3, Et) \Rightarrow \{C/C3/-\,H/O/O\},$$

$$CH_4 + O \rightarrow CH_3 + OH \Rightarrow \{C/H3/-\,H/O\},$$

$$RCH_3 + O \rightarrow RCH_2 + OH (R = CH_3, Et, Pr, i\text{-}Pr, t\text{-}Bu) \Rightarrow \{C/C/H2/-\,H/O\},$$

$$CH_3OX + H \rightarrow CH_2OX + H_2 \quad \{X = H, Me, i\text{-}Pr, t\text{-}Bu, OH, CHO, COCH_3\} \Rightarrow \{C/O/H2/-\,H/H\},$$

and in each case they are generalized to give rate-estimation rules.

Our rate-estimation method appears to be limited to reaction families with well-determined TS and primarily by the accuracy of the high-level quantum chemical PES

calculations on which it is based. Certainly this is true in cases such as the peroxyl radical and O atom reactions studied here where conventional quantum chemistry techniques are known to have some difficulty.

The TS GA method has the advantage that the supergroup value can easily be refined to make better generic rate prediction when experimental data become available on even a single reaction belonging to that family. Often errors in quantum chemical methods are systematic in nature and are identifiable with specific interactions in the system. This behavior aids immensely in the proper choice of a quantum chemical method for the system of interest. In certain cases other approximations in the rate calculation contribute significantly to the error. Efficient approximate methods exist for converting the $k_\infty(T)$ computed using this method (and most rate-estimation methods in the literature) into $k(T,P)$ for comparison with experiment, though these can also introduce modest errors. By generalizing from small-molecule reactions to larger homologues, the new method provides an effective way to derive considerable benefit from each expensive quantum chemical calculation and from each improvement in rate-calculation technology.

Acknowledgements. This work was partially supported by the National Computational Science Alliance under Grant CTS010006 N and utilized the Origin 2000 High-performance Computing and UniTree Mass Storage systems. We are grateful for financial support from the EPA Center for Airborne Organics, the NSF CAREER program, Alstom Power, Dow Chemical, and the Office of Basic Energy Science, U.S. Department of Energy through grant DE-FG02-98ER14914. The authors acknowledge the contribution of Hans-Heinrich Carstensen in the initial stages of this work.

References

1. Hammett LP (1940) Physical organic chemistry. Mc Graw-Hill, New York
2. Benson SW (1976) Thermochemical kinetics. Wiley, New York
3. Miller WH (1998) J Phys Chem A 102:793
4. Truhlar DG, Isaacson AD, Garrett BC (1985) Theory of chemical reaction dynamics. CRC, Boca Raton
5. Brown PN, Byrne GD, Hindmarsh AC (1989) SIAM J Sci Stat Comput 10:1038
6. Petzold LR (1983) Scientific computing. North-Holland, Amsterdam
7. Kee RJ, Miller JA, Jefferson TH (1980) CHEMKIN Sandia National Laboratories, Livermore, CA
8. Susnow RG, Dean AM, Green WH, Peczak P, Broadbelt LJ (1997) J Phys Chem A 101:3731
9. Broadbelt LJ, Stark SM, Klein MT (1994) Ind Eng Chem Res 33:790
10. Broadbelt LJ, Stark SM, Klein MT (1995) Ind Eng Chem Res 34:2566
11. Broadbelt LJ, Stark SM, Klein MT (1996) Comput Chem Eng 20:113
12. Klinke DJ, Broadbelt LJ (1997) AIChE J 43:1828
13. Klinke DJ, Broadbelt LJ (1999) Chem Eng Sci 54:3379
14. DeWitt MJ, Dooling DJ, Broadbelt LJ (2000) Ind Eng Chem Res 39:2228
15. Chevalier C, Warnatz J, Melenk H (1990) Ber Bunsenges Phys Chem 94:1362
16. Chevalier C, Pitz WJ, Warnatz J, Westbrook CK, Melenk H (1992) Proc Combust Inst 24:93
17. Hillewaert LP, Diericks JL, Froment GF (1988) AIChE J 34:17
18. DiMaio FP, Lignola PG (1992) Chem Eng Sci 47:2713
19. Prickett SE, Mavrovouniotis ML (1997) Comput Chem Eng 21:1219
20. Prickett SE, Mavrovouniotis ML (1997) Comput Chem Eng 21:1237
21. Prickett SE, Mavrovouniotis ML (1997) Combust Sci Technol 21:1325
22. Mavrovouniotis ML, Prickett SE (1998) Knowledge-Based Syst 10:199
23. Mavrovouniotis ML, Constantinou E, Prickett SE (1992) 3rd IFAC symposium. Pergamon, New York
24. Blurock ES (1995) J Chem Inf Comput Sci 35:607
25. Warth V, Battin-Leclerc F, Fournet R, Glaude PA, Come GM, Scacchi G (2000) Comput Chem 24:541
26. Fournet R, Warth V, Glaude PA, Battin-Leclerc F, Scacchi G, Come GM (2000) Int J Chem Kinet 32:36
27. Glaude PA, Warth V, Fournet R, Battin-Leclerc F, Scacchi G, Come GM (1998) Int J Chem Kinet 30:949
28. Warth V, Stef N, Glaude PA, Battin-Leclerc F, Scacchi G, Come GM (1998) Combust Flame 114:81
29. Muller C, Scacchi G, Come GM (1991) Comput Chem 15:337
30. Come GM, Warth V, Glaude PA, Fournet R, Battin-Leclerc F, Scacchi G (1996) Proc Combust Inst 26:755
31. Bounaceur R, Warth V, Glaude PA, Battin-Leclerc F, Scacchi G, Come GM, Faravelli T, Ranzi E (1996) J Chim Phys 93:1472
32. Glaude PA, Battin-Leclerc F, Judenherc B, Warth V, Fournet R, Come GM, Scacchi G (2000) Combust Flame 121:345
33. Glaude PA, Warth V, Fournet R, Battin-Leclerc F, Come GM, Scacchi G (1997) Bull Soc Chim Belg 106:343
34. Battin-Leclerc F, Glaude PA, Warth V, Fournet R, Scacchi G, Come GM (2000) Chem Eng Sci 55:2883
35. Ranzi E, Faravelli T, Gaffuri P, Pennati G, Westbrook CK, Pitz WJ (1995) Combust Flame 99:201
36. Tomlin AS, Turanyi T, Pilling MJ (1997) Low temperature combustion and autoignition. Elsevier, Amsterdam
37. Matheu DM, Lada TA, Green WH, Jr., Dean AM, Grenda JM (2001) Comput Phys Commun 138: 237
38. Grenda JM, Dean AM, Peczak P, Green WH Jr (1998) 27th symposium (international) on combustion. Boulder, CO
39. Grenda JM, Bozzelli JW, Dean AM (2000) 8th international conference on numerical combustion, CP4. Amelia Island, FL
40. Green WH Jr, Barton PI, Bhattacharjee B, Matheu DM, Schwer DA, Song J, Sumathi R, Carstensen H-H, Dean AM, Grenda JM (2001) Ind Eng Chem Res 40:5362
41. Truong TN, Duncan WT, Tirtowidjojo M (1999) Phys Chem Chem Phys 1:1061
42. Truong TN (2000) J Chem Phys 113:4957
43. Pople JA, Head-Gordon M, Fox DJ, Raghavachari K, Curtiss LA (1989) J Chem Phys 90:5622
44. Curtiss LA, Jones C, Trucks GW, Raghavachari K, Pople JA (1990) J Chem Phys 93:2537
45. Curtiss LA, Raghavachari K, Trucks GW, Pople JA (1991) J Chem Phys 94:7221
46. Curtiss LA, Raghavachari K, Pople JA (1993) J Chem Phys 98:1293
47. Curtiss LA, Raghavachari K, Redfern PC, Rassolov V, Pople JA (1998) J Chem Phys 109:7764
48. Curtiss LA, Redfern PC, Raghavachari K, Rassolov V, Pople JA (1999) J Chem Phys 110:4703
49. Baboul AG, Curtiss LA, Redfern PC, Raghavachari K (1999) J Chem Phys 110:7650
50. Curtiss LA, Raghavachari K, Redfern PC, Pople JA (2000) J Chem Phys 112:1125
51. Ochterski JW, Petersson GA, Montgomery JA Jr (1996) J Chem Phys 104:2598
52. Montgomery JA Jr, Ochterski JW, Petersson GA (1994) J Chem Phys 101:5900
53. Mayer PM, Parkinson CJ, Smith DM, Radom L (1998) J Chem Phys 108:604
54. Montgomery JA Jr, Frisch MJ, Ochterski JW, Petersson GA (1999) J Chem Phys 110:2822

55. Fast PL, Corchado JC, Sanchez ML, Truhlar DG (1999) J Phys Chem A 103:5129
56. Fast PL, Schultz NE, Truhlar DG (2001) J Phys Chem A 105:4143
57. Lynch BJ, Truhlar DG (2002) J Phys Chem A 106:842
58. Fast PL, Truhlar DG (2000) J Phys Chem 104:6111
59. Fast PL, Sanchez ML, Corchado JC, Truhlar DG (1999) J Chem Phys 110:11679
60. Fast PL, Sanchez ML, Truhlar DG (1999) Chem Phys Lett 306:407
61. Parr R, Yang W (1989) Density-functional theory of atoms and molecules. Oxford University Press, New York
62. Lynch BJ, Fast PL, Harris M, Truhlar DG (2000) J Phys Chem A 104:4811
63. Pople JA, Gordon MH, Raghavachari K (1987) J Chem Phys 87:5968
64. Andersson K, Borowki P, Fowler PW, Malmqvist P-A, Roos BO, Sadlej AJ (1992) Chem Phys Lett 190:367
65. Werner H-J, Knowles PJ (1988) J Chem Phys 89:5803
66. Knowles PJ, Werner H-J (1988) Chem Phys Lett 145:514
67. Martin JML, de Oliveira G (1999) J Chem Phys 111:1843
68. Parthiban S, de Oliveira G, Martin JML (2001) Understanding chemical reactivity series. Kluwer, Dordrecht, The Netherlands
69. Becke AD (1997) J Chem Phys 107:8554
70. Tozer DJ, Handy NC, Green WH (1997) Chem Phys Lett 273:183
71. Tozer DJ, Handy NC (1998) J Chem Phys 108:2545
72. Tozer DJ, Handy NC (1998) J Phys Chem A 102:3162
73. Hampbrecht FA, Cohen AJ, Tozer DJ, Handy NC (1998) J Chem Phys 109:6264
74. Malick DK, Petersson GA, Montgomery JA Jr (1998) J Chem Phys 108:5704
75. Pitzer KS, Gwinn WD (1942) J Chem Phys 10:428
76. Pitzer KS (1946) J Chem Phys 14:239
77. Kilpatrick JE, Pitzer KS (1943) J Chem Phys 11:1064
78. Gang J, Pilling MJ, Robertson SH (1996) J Chem Soc Faraday Trans 92:3509
79. Truhlar DG (1991) J Comput Chem 12:266
80. McClurg RB, Flagan RC, Goddard WA (1997) J Chem Phys 106:6675
81. Ayala PY, Schlegel HB (1998) J Chem Phys 108:2314
82. Mazyar O, Green WH Jr (in preparation)
83. East ALL, Radom L (1997) J Chem Phys 106:6655
84. Johnson PM, Sears TJ (1999) J Chem Phys 111:9222
85. Carter S, Bowman JM, Handy N (1998) Theor Chem Acc 100:191
86. Eyring H (1935) J Chem Phys 3:107
87. Eyring H (1938) Trans Faraday Soc 34:41
88. Glasstone S, Laidler KJ, Eyring H (1941) The theory of rate processes. McGraw-Hill, New York
89. Hirschfelder JO, Wigner E (1939) J Chem Phys 7:616
90. Lu DH, Truong TN, Melissas VS, Lynch GC, Liu YP, Garrett BC, Steckler R, Isaacson AD, Rai SN, Hancock GC, Lauderdale JG, Joseph T, Truhlar DG (1992) Comput Phys Commun 71:235
91. Truong TN, Truhlar DG (1990) J Chem Phys 93:1761
92. Villa J, Truhlar DG (1997) Theor Chem Acc 97:317
93. Truhlar DG, Garrett BC (1980) Acc Chem Res 13:440
94. Truhlar DG, Garrett BC, Klippenstein SJ (1996) J Phys Chem 100:12771
95. Steckler R, Hu W-P, Liu Y-P, Lynch GC, Garrett BC, Isaacson AD, Melissas VS, Lu D-H, Truong TN, Rai SN, Hancock GC, Lauderdale JG, Joseph T, Truhlar DG (1995) Comput Phys Commun 88:341
96. Corchado JC, Chuang Y-Y, Fast PL, Villa J, Hu W-P, Liu Y-P, Lynch GC, Nguyen KA, Jackels CF, Melissas VS, Lynch BJ, Rossi I, Coitino EL, Fernandez-Ramos A, Pu J, Steckler R, Garrett BC, Isaacson AD, Truhlar DG (2002) POLYRATE 8.7.2. Minneapolis, MN 55455
97. Duncan WT, Bell RL, Truong TN (1998) J Comput Chem 19:1039
98. Klippensterin SJ, Wagner AF, Robertson SH, Dunbar RC, Wardlaw DM (1999) http://chemistry.anl.gov/chem-dyn/VariFlex 1.0. Argonne National Laboratory, Argonne, IL
99. Viel A, Leforestier C, Miller WH (1998) J Chem Phys 108:3489
100. Skinner DE, Germann TC, Miller WH (1998) J Phys Chem A 102:3828
101. Wang H, Thompson WH, Miller WH (1998) J Phys Chem A 102:9372
102. Klippenstein SJ, Harding LB (2000) J Phys Chem A 104: 2351
103. Miller WH (1998) Faraday Discuss Chem Soc 110:1
104. Albu TV, Corchado JC, Truhlar DG (2001) J Phys Chem A 105:8465
105. Gorin E (1938) Acta Physicochim URSS 9:681
106. Nikitin EE (1965) Theor Exp Chem 1:83
107. Pechukas P, Light JC (1965) J Chem Phys 42:3281
108. Quack M, Troe J (1974) Ber Bunsenges Phys Chem 78:240
109. Quack M, Troe J (1975) Ber Bunsenges Phys Chem 79:170
110. Green WH Jr, Moore CB, Polik WF (1992) Annu Rev Phys Chem 43:591
111. Klippenstein SJ, East ALL, Allen WD (1996) J Chem Phys 105:118
112. Knyazev VD, Tsang W (1999) J Phys Chem A 103:3944
113. Gilbert RG, Smith SC (1990) Theory of unimolecular and recombination reactions. Blackwell, Oxford.
114. Holbrook KA, Pilling MJ, Robertson SH (1996) Unimolecular reactions. Wiley, New York
115. Forst W (1973) Theory of unimolecular reactions. Academic, New York
116. Barker JR (2001) Int J Chem Kinet 33:232
117. Vereecken L, Huyberechts G, Peeters J (1997) J Chem Phys 106:6564
118. Ritter ER and Bozzelli JW (1991) Int J Chem Kinet 23: 767
119. Lay TH, Bozzelli JW, Dean AM, Ritter ER (1995) J Phys Chem 99:15054
120. Ritter ER, Bozzelli JW (1991) Int J Chem Kinet 23:767
121. Grenda JM, Bozzelli JW (2000) GAPP (group additivity property predictor, version 1.0. ExxonMobil Research and Engineering Company, Annandale, NJ
122. Forst W (1972) J Phys Chem 76:342
123. Dean AM (1985) J Phys Chem 89:4600
124. Troe J (1977) J Chem Phys 66:4758
125. Matheu DM, Grenda JM, Green WH Jr (2002) Int J Chem Kinet (submitted)
126. Johnston HS (1966) Gas phase reaction rate theory. Ronald, New York
127. Evans MG, Polanyi M (1938) Trans Faraday Soc 34:1
128. Butler ET, Polanyi M (1943) Trans Faraday Soc 39:19
129. Hinshelwood CN, Laidler K, Timm EW (1938) J Chem Soc 848
130. Semenov NN (1958) Some problems in chemical kinetics and reactivity. Pergamon, London
131. Taft RW (1952) J Am Chem Soc 74:2729
132. Pilling MJ, Seakins PW (1995) Reaction kinetics. Oxford University Press, Oxford
133. Marcus RA (1956) J Chem Phys 24:966
134. Marcus RA (1968) J Phys Chem 72:891
135. Cogen AO, Marcus RA (1968) J Phys Chem 72:4249
136. Johnston HS, Parr C (1963) J Am Chem Soc 85:2544
137. Xing SB, Shi SH, Qui LX (1992) Int J Chem Kinet 24:1
138. Qui LX, Shi SH, Xing SB, Chen XG (1992) J Phys Chem 96:685
139. Tribert J, Meinike T, Olzmann M, Scherzer K (1995) Z Phys Chem 191:47
140. Su MC, Lim KP, Michael JV, Hranisavljevic J, Xun YM, Fontijn A (1994) J Phys Chem 98:8411
141. Denisov ET (1999) General aspects of the chemistry of radicals. Wiley, New York
142. Zavitsas AA (1972) J Am Chem Soc 94:2779

143. Zavitsas AA, Melikian AA (1975) J Am Chem Soc 97:2757
144. Zavitsas AA, Chatgilialoglu C (1995) J Am Chem Soc 117:10645
145. Berces T, Dombi J (1980) Int J Chem Kinet 12:183
146. Shustorovich E (1990) Adv Catal 37:101
147. Kagiya T, Sumida Y, Inone T, Dyachkovskii FS (1696) Bull Chem Soc Jpn 42:1812
148. Kagiya T, Sumida Y, Inone T (1969) Bull Chem Soc Jpn 42:2422
149. Rudakov ES, Volkova LK (1978) Dokl Akad Nauk UKR Ser B 10:912
150. Berkowitz M, Parr RG (1998) J Chem Phys 88:2554
151. Yang W, Parr RG (1985) Proc Natl Acad Sci USA 82:6723
152. Gaffney JS, Levine SZ (1979) Int J Chem Kinet 11:1197
153. Atkinson R (1980) Int J Chem Kinet 12:761
154. Guesten H, Klasinc L (1986) Naturwissenschaften 73:129
155. Atkinson R, Pitts JN (1977) J Chem Phys 67:2492
156. Canosa-Mas E, Monks PS, Wayne RP (1992) J Chem Soc Faraday Trans 88:11
157. Niiranen JT, Gutman D (1993) J Phys Chem 97:4106
158. Masaki A, Tsunashima S, Washida N (1995) J Phys Chem 99:13126
159. Paltenghi R, Ogryzlo EA, Bayes KD (1984) J Phys Chem 88:2595
160. Marston G, Monks PS, Canosa-Mas CE, Wayne RP (1993) J Chem Soc Faraday Trans 89:3899
161. Krech RH, McFadden DL (1977) J Am Chem Soc 99:8402
162. Krech RH, Diebold GJ, McFadden DL (1977) J Am Chem Soc 99:4605
163. Alfassi ZB, Benson SW (1973) Int J Chem Kinet 5:879
164. Atkinson R (1986) Chem Rev 85:69
165. Sabljic A, Guesten H (1990) Atmos Environ 24A:73
166. Grosjean D, Williams EL (1992) Atmos Environ 26A:1395
167. Canosa-Mas CE, Smith SJ, Toby S, Wayne RP (1988) J Chem Soc Faraday Trans II 84:247
168. Aird RWS, Canosa-Mas CE, Cook DJ, Ljuengstron E, Marston G, Monks PS, Wayne RP (1992) J Chem Soc Faraday Trans 88:1093
169. Atkinson R (1987) Int J Chem Kinet 19:799
170. Atkinson R (1988) Environ Toxicol Chem 7:435
171. Kwok ESC, Atkinson R (1995) Atmos Environ 29:1685
172. DeMore WB (1996) J Phys Chem 100:5813
173. Bakken GA, Jurs PC (1999) J Chem Inf Comput Sci 39:508
174. Blowers P, Ford L, Masel RI (1998) J Phys Chem A 102:9267
175. Blowers P, Masel RI (1998) J Phys Chem A 102:9957
176. Lee WT, Masel RI (1998) J Phys Chem A 102:2332
177. Blowers P, Masel RI (2000) Theor Chem Acc 105:46
178. Klamt A (1993) Chemosphere 26:1273
179. Klamt A (1996) Chemosphere 32:717
180. Golden DM (1981) Modelling of chemical reaction systems. Springer, Berlin Heidelberg New York
181. Benson SW, Cruickshank FR, Golden DM, Haugen GR, O'Neal HE, Rodgers AS, Shaw R, Walsh R (1979) Chem Rev 69:279
182. Cohen N (1991) Int J Chem Kinet 23:397
183. Cohen N (1991) Int J Chem Kinet 23:683
184. Cohen N (1982) Int J Chem Kinet 14:1339
185. Ranzi E, Dente M, Faravelli T, Pennati G (1994) Combust Sci Technol 95:1
186. Sumathi R, Carstensen H-H, Green WH Jr (2001) J Phys Chem A 105:6910
187. Sumathi R, Carstensen H-H, Green WH Jr (2001) J Phys Chem A 105:8969
188. Sumathi R, Carstensen H-H, Green WH Jr (2002) J Phys Chem A 106: 5474
189. Frisch MJ, Trucks GW, Schlegel HB, Scuseria GE, Robb MA, Cheeseman JR, Zakrzewski VG, Montgomery JA, Stratmann RE, Burant JC, Dapprich S, Millam JM, Daniels AD, Kudin KN, Strain MC, Farkas O, Tomasi J, Barone V, Cossi M, Cammi R, Mennucci B, Pomelli C, Adamo C, Clifford S, Ochterski J, Petersson GA, Ayala PY, Cui Q, Morokuma K, Malick DK, Rabuck AD, Raghavachari K, Foresman JB, Cioslowski J, Ortiz JV, Baboul AG, Stefanov BB, Liu G, Liashenko A, Piskorz P, Komaromi I, Gomperts R, Martin AL, Fox DJ, Keith T, Al-Laham MA, Peng CY, Nanayakkara A, Challacombe M, Gill PMW, Johnson B, Chen W, Wong MW, Andres JL, Gonzalez C, Head-Gordon M, Replogle ES, Pople JA (1998) Gaussian 98, revision A.9. Gaussian, Pittsburg, PA
190. Nicolaides A, Rauk A, Glukhovtsev MN, Radom L (1996) J Phys Chem 100:17460
191. Petersson GA, Malick DK, Wilson WG, Ochterski JW, Montgomery JA Jr, Frisch MJ (1998) J Chem Phys 109:10570
192. Shum LGS, Benson SW (1983) J Phys Chem 87:3479
193. Howard CJ (1980) J Am Chem Soc 102:6937
194. Kondo O, Benson SW (1984) J Phys Chem 88:6675
195. Lay TH, Bozzelli JW (1997) J Phys Chem A 101:9505
196. Johnson BG, Gonzales CA, Gill PMW, Pople JA (1994) Chem Phys Lett 221:100
197. Zhang Q, Bell R, Truong TN (1995) J Phys Chem 99:592
198. Hrusak J, Friedrichs H, Schwarz H, Razafinjanahary H, Chermette H (1996) J Phys Chem 100:100
199. Baker J, Muit M, Andzelm J (1995) J Chem Phys 102:2063
200. Baker J, Andzelm J, Muir M, Taylor PR (1995) Chem Phys Lett 237:53
201. Nguyen MT, Creve S, Vanquickenborne LG (1996) J Phys Chem 100:18422
202. Chatgilaloglu C, Dickhaut J, Giese B (1991) J Org Chem 56:6399
203. Chatgilaloglu C, Ingold KU, Scaiano JC (1981) J Am Chem Soc 103:7739
204. Berkowitz J, Ellison GB, Gutman D (1994) J Phys Chem 102:10787
205. Smith BJ, Radom L (1998) J Phys Chem A 102:10787
206. Jursic BS (1997) Int J Quantum Chem 65:75
207. Jursic BS (1998) J Mol Struct (THEOCHEM) 427:137
208. Corchado JC, Espinosa-Garcia J, Roberto-Neto O, Chuang Y-Y, Truhlar DG (1998) J Phys Chem A 102:4899
209. Walker RW (1977) Gas kinetics and energy transfer. Specialist periodical report. Chemical Society, London, p 296
210. Baldwin RR, Hisham MWH, Keen A, Walker RW (1982) J Chem Soc Faraday Trans I 78:1165
211. Tsang W, Hampson RF (1986) J Phys Chem Ref Data 15:1087
212. Tsang W (1987) J Phys Chem Ref Data 16:471; ibid, (1988) 17:887
213. Baulch DL, Cobos CJ, Cos RA, Esser C, Frank P, Just T, Kerr JA, Pilling MJ, Troe J, Walker RW, Warnatz J (1992) J Phys Chem Ref Data 21:411
214. NIST Chemical Kinetics Database, version 2Q98, Standard Reference Data Program, NIST, Gaithersburg, MD
215. Curran HJ, Gaffuri P, Pitz WJ, Westbrook CK (1998) Combust Flame 114:149
216. Hughes KJ, Turanyi T, Clague A, Pilling MJ (2001) Int J Chem Kinet 33:513
217. Konnov AA (2001) http://homepages.vub.ac.be/~akonnov/
218. Hidaka Y, Nishimori T, Sato K, Henmi Y, Okuda R, Inami K (1999) Combust Flame 117:755
219. Miller JA, Bowman CT (1989) Prog Energy Combust Sci 15:287
220. Ranzi E, Sogardo A, Gaffuri P, Pennati G, Faravelli T (1994) Combust Sci Technol 96:279
221. Miyoshi A, Tsuchiya K, Yamaguchi N, Matsui N (1994) J Phys Chem 98:11452
222. Cohen N, Westberg KR (1986) Int J Chem Kinet 18:99
223. Cohen N, Westberg KR (1991) J Phys Chem Ref Data 20: 1211
224. Smith GP, Golden DM, Frenklach M, Moriarty NW, Eiteneer B, Goldenberg M, Bowman T, Hanson RK, Song S, Gardiner WC, Lissianski VV, Zhiwei Q (2000) GRI Mech 3.0. http://www.me.berkeley.edu/gri-mech/
225. Marinov NM, Malte PC (1995) Int J Chem Kinet 27:957